

# 1 Observations of recent Arctic sea ice volume loss and its impact 2 on ocean-atmosphere energy exchange and ice production

3 N. T. Kurtz,<sup>1,2</sup> T. Markus,<sup>2</sup> S. L. Farrell,<sup>2,3</sup> D. L. Worthen,<sup>2,4</sup> and L. N. Boisvert<sup>2,5</sup>

4 Received 2 March 2010; revised 3 December 2010; accepted 27 January 2011; published XX Month 2011.

5 [1] Using recently developed techniques we estimate snow and sea ice thickness  
6 distributions for the Arctic basin through the combination of freeboard data from the  
7 Ice, Cloud, and land Elevation Satellite (ICESat) and a snow depth model. These data  
8 are used with meteorological data and a thermodynamic sea ice model to calculate  
9 ocean-atmosphere heat exchange and ice volume production during the 2003–2008 fall and  
10 winter seasons. The calculated heat fluxes and ice growth rates are in agreement with  
11 previous observations over multiyear ice. In this study, we calculate heat fluxes and ice  
12 growth rates for the full distribution of ice thicknesses covering the Arctic basin and  
13 determine the impact of ice thickness change on the calculated values. Thinning of the sea  
14 ice is observed which greatly increases the 2005–2007 fall period ocean-atmosphere heat  
15 fluxes compared to those observed in 2003. Although there was also a decline in sea  
16 ice thickness for the winter periods, the winter time heat flux was found to be less impacted by  
17 the observed changes in ice thickness. A large increase in the net Arctic ocean-atmosphere  
18 heat output is also observed in the fall periods due to changes in the areal coverage of  
19 sea ice. The anomalously low sea ice coverage in 2007 led to a net ocean-atmosphere heat  
20 output approximately 3 times greater than was observed in previous years and suggests that  
21 sea ice losses are now playing a role in increasing surface air temperatures in the Arctic.

22 **Citation:** Kurtz, N. T., T. Markus, S. L. Farrell, D. L. Worthen, and L. N. Boisvert (2011), Observations of recent Arctic sea ice  
23 volume loss and its impact on ocean-atmosphere energy exchange and ice production, *J. Geophys. Res.*, 116, XXXXXX,  
24 doi:10.1029/2010JC006235.

## 25 1. Introduction

26 [2] Recent observations have shown a decline in Arctic  
27 sea ice areal coverage, freeboard, thickness, and volume  
28 [e.g., *Stroeve et al.*, 2008; *Farrell et al.*, 2009; *Rothrock*  
29 *et al.*, 2008; *Giles et al.*, 2008; *Kwok et al.*, 2009] along  
30 with widespread environmental and climatic changes in the  
31 Arctic [*Arctic Climate Impact Assessment*, 2005]. These  
32 changes to the sea ice system have the potential to impact  
33 the Arctic climate by altering the radiation and heat budgets  
34 of the ocean and atmosphere. The degree to which the cold  
35 Arctic atmosphere is insulated from the relatively warm ocean  
36 is affected by the presence of a sea ice cover; the ocean-  
37 atmosphere heat flux can vary by nearly 2 orders of magnitude  
38 between open water and an ocean covered with thick sea ice  
39 for winter time conditions [*Maykut*, 1978]. This insulating

effect of sea ice makes the Arctic much colder than is typical of 40  
a maritime environment. The exchange of heat between the 41  
ocean and the atmosphere is also responsible for the growth 42  
of sea ice as heat lost from the ocean to the atmosphere is 43  
balanced by ice production. With thinner ice comes more 44  
heat exchange and faster ice growth which could potentially 45  
slow or reverse the observed losses in ice thickness. 46

[3] The loss of sea ice may play a role in Arctic ampli- 47  
fication, wherein the Arctic region is expected to see a much 48  
greater share of warming as worldwide temperatures increase 49  
[*Manabe and Stouffer*, 1980]. Modeling studies show that 50  
decreases in sea ice thickness and its areal coverage lead to 51  
increased ocean-atmosphere heat transfer. Due to the strong 52  
stratification of the Arctic atmosphere this heat is trapped 53  
near the surface leading to increased surface air temperatures 54  
[*Boé et al.*, 2009]. In addition to modeling studies, observa- 55  
tions from buoy data have suggested that thinning of the sea 56  
ice cover during the 1979–1998 time period led to increases 57  
in surface air temperature through an increase in the ocean- 58  
atmosphere heat flux [*Rigor et al.*, 2002]. There remains, 59  
however, much uncertainty into how large a role recent 60  
changes in the sea ice cover have, and will continue to play, 61  
with regard to Arctic warming. Using reanalysis data, *Serreze* 62  
*et al.* [2009] found that losses in sea ice areal coverage have 63  
played a role in autumn surface air temperature increases in 64  
the Arctic. They also found that a winter warming signal may 65  
be beginning to emerge which they hypothesize may be due 66

<sup>1</sup>Joint Center for Earth Systems Technology, University of Maryland  
Baltimore County, Baltimore, Maryland, USA.

<sup>2</sup>Hydrospheric and Biospheric Sciences Laboratory, NASA Goddard  
Space Flight Center, Greenbelt, Maryland, USA.

<sup>3</sup>Cooperative Institute for Climate Studies, Earth System Science  
Interdisciplinary Center, University of Maryland, College Park, Maryland,  
USA.

<sup>4</sup>RS Information Systems, McLean, Virginia, USA.

<sup>5</sup>Department of Atmospheric and Oceanic Sciences, University of  
Maryland, College Park, Maryland, USA.

**Table 1.** Input Parameters Used in This Study and Their Sources

Symbol	Description	Source
$T_a$	2 m air temperature	ECMWF
$T_d$	2 m dew point temperature	ECMWF
$p_0$	surface pressure	ECMWF
$u$	10 m wind speed	ECMWF
$Cl$	cloud fraction	MODIS
$T_w$	sea surface temperature	AMSR-E
$h_s$	snow depth	snow model
$h_f$	freeboard	ICESat
$h_i$	ice thickness	ICESat freeboard with snow model

to delays in autumn freezeup and decreased ice extent and thickness in the winter. However, a major limitation in studies such as these has been the lack of a high-resolution, basin-wide sea ice thickness observational data set with which to adequately study the impact of sea ice thickness changes on the Arctic energy budget.

[4] Recent satellite altimetry missions have provided the capability of obtaining basin-wide Arctic sea ice thickness measurements. In this paper, we use laser altimetry data from NASA's Ice, Cloud, and land Elevation Satellite (ICESat) to estimate sea ice freeboard across the Arctic basin. The freeboard data are then combined with a snow depth model to estimate sea ice and snow thickness values for the Arctic at the high spatial resolution needed for studying the impact of sea ice on the energy budget. The sea ice thickness data are used with meteorological data and a thermodynamic sea ice model to study the impact of sea ice thickness changes on the ocean-atmosphere heat flux and ice growth rate over the 2003–2008 time period when significant changes to the Arctic sea ice cover took place.

[5] The meteorological forcings, as well as the data sets and methodologies used to derive the sea ice thickness and snow depth are described in section 2. Section 3 describes the thermodynamic model used for determining the heat transfer through the ocean-ice-atmosphere system and calculating the ice growth rate. The calculated heat fluxes, ice growth rates, and uncertainties are presented in section 4 and compared to results from previous studies. The role of observed thinning of the ice and snow covers in increasing the ocean-atmosphere heat flux is also discussed. Section 5 expands the analysis to the full Arctic Ocean including nonice-covered regions. Section 6 summarizes the main conclusions of our study.

## 2. Data Sets

[6] In this section, we provide a description of the data sets and methods used to derive snow depth, sea ice thickness, and the meteorological parameters used in our analysis. These data sets are used in the following section to calculate the ocean-atmosphere heat flux and ice growth rate. No single sensor provides the requisite data, thus a combination of observation, model, and assimilated data is used. Table 1 provides a summary of the input data sets with detailed descriptions provided below. Error estimates for each data set, along with the propagation of these errors into the calculated heat flux and ice growth rate, are addressed in section 5. We restrict our data set to the Arctic Ocean region shown in the shaded region of Figure 1 to avoid mixing high- and low-latitude sea ice regions in the analysis.

## 2.1. Meteorological Data

[7] Reanalysis data from the European Center for Medium-Range Weather Forecasts (ECMWF) ERA-Interim data set are used to provide the 2 m air temperature, 2 m dew point temperature, 10 m wind speed, surface pressure, and snowfall. ERA-Interim combines observational and model data into an assimilated data set using the 4D-VAR method. Data is provided at 6 h time intervals with a spatial resolution of 1.5° latitude by 1.5° longitude.

[8] Cloud fraction is taken from the daily Moderate Resolution Imaging Spectroradiometer (MODIS) 1° × 1° global gridded product. A correction factor of 0.1 has been added to all cloud fraction data to account for a bias in the Arctic region of the data set [Ackerman et al., 2008]. Cloud fractions from MODIS, rather than ECMWF are used because of the anomalously high values found in the ECMWF data for this time period; the ECMWF cloud fractions were found to be approximately 30–40% higher than those from previously published observations [e.g., Lindsay, 1998].

[9] Sea surface temperatures are classified as the temperature of the top layer of water approximately 1 millimeter thick. They are taken from the daily 0.25° by 0.25° gridded product derived from ten-channel Advanced Microwave Scanning Radiometer–Earth Observing System (AMSR-E) brightness temperature data [Wentz and Meissner, 2004]. These sea surface temperatures are provided for ice-free areas to within 75 km of coastlines. The estimated error in the sea surface temperatures is 0.58 K [Wentz and Meissner, 2000].

## 2.2. Snow Model

[10] Snow depth on sea ice is modeled using a domain defined by the 25 km AMSR-E grid. Snow depth on the model grid is determined by

$$\frac{\partial S}{\partial t} = -\nabla \cdot (V \cdot S) + a_i \frac{\rho_s}{\rho_w} F,$$

where  $S$  is the average snow thickness in a grid cell (including both open water and ice covered areas),  $V$  is the

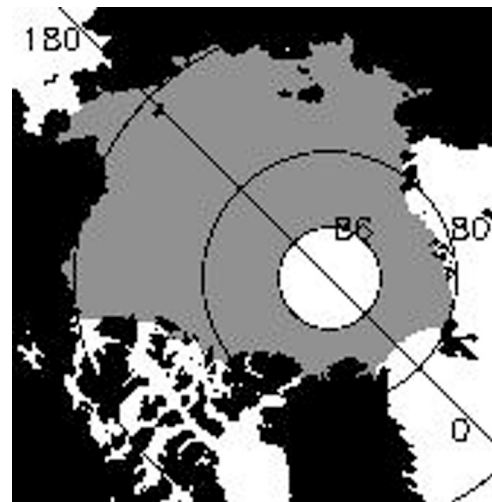


**Figure 1.** Map of the region used in the analysis. The shaded region is defined as the Arctic Ocean in this study.

**Table 2.** Time Periods Used in This Analysis Based on the Availability of ICESat Data<sup>a</sup>

Campaign Name	Period	Days of Operation
ON03	Oct 1 to Nov 18 2003	49
ON03_1	Oct 1 to Nov 8 2003	39
ON03_2	Oct 15 to Nov 18 2003	35
FM04	Feb 17 to Mar 21 2004	34
ON04	Oct 3 to Nov 8 2004	37
FM05	Feb 17 to Mar 24 2005	36
ON05	Oct 21 to Nov 24 2005	35
FM06	Feb 22 to Mar 27 2006	34
ON06	Oct 25 to Nov 27 2006	34
MA07	Mar 12 to Apr 14 2007	34
ON07	Oct 2 to Nov 5 2007	37
FM08	Feb 17 to Mar 21 2008	34

<sup>a</sup>The ON03 campaign has been subdivided into two campaigns, ON03\_1 and ON03\_2, for better temporal comparison with other fall ICESat campaigns.

ice velocity vector,  $a_i$  is the ice concentration,  $\rho_s$  is the snow density,  $\rho_w$  is the density of water, and  $F$  is the snowfall (in snow water equivalent). The snow depth is initialized each year on 15 September before the summer minimum sea ice extent, the initial snow cover on multiyear ice and the snow density values are taken from the climatology of Warren *et al.* [1999]. The daily AMSR-E sea ice concentrations at each grid point are specified at the start of each day and remain constant throughout the day. Daily snowfall at each model grid point is estimated using the liquid water equivalent from the ECMWF ERA-Interim reanalysis data similar to the method used by Kwok and Cunningham [2008]. Ice velocity for each grid point is determined from AMSR-E 89 GHz data using the wavelet analysis algorithm of Liu and Cavalieri [1998]. The model is run each year during the fall through spring periods to estimate the snow depth over the time period covering each ICESat measurement campaign.

### 2.3. ICESat Data

[11] ICESat measures the surface elevation using a 1064 nm laser altimeter [Zwally *et al.*, 2002]. Spatial coverage of the Arctic Ocean is provided up to 86°N with a 170 m shot-to-shot spacing and a footprint size of approximately 70 m. The cloud filtering parameters described by Kwok *et al.* [2007] are first used to filter out low-quality data which has been affected by atmospheric forward scattering. The elevation data from ICESat are used to determine the sea ice freeboard,  $h_f$ , which is here defined as the height of the snow and ice layer above the local sea surface. Freeboard data is collected only in areas where the ice concentration determined from AMSR-E is greater than 30%. The ICESat data products are of Release 428, which include orbit and attitude determination as well as detector saturation corrections for the time periods studied here. Freeboard is found from the ICESat elevation data through the use of sea surface tie points following the method of Kwok *et al.* [2007]. [12] Due to the approximately 70 m footprint size of ICESat, some sea surface tie points used in the retrieval of freeboard from ICESat data are expected to be biased due to contamination of snow and ice within the footprint. Comparisons of ICESat data with coincident high-resolution airborne laser altimetry data have shown this can be problematic with a freeboard bias of up to 9 cm observed in one study

[Kurtz *et al.*, 2008]. Corrections to account for biases due to snow and ice within sea surface tie point footprints have been proposed by Kwok and Cunningham [2008] and Kwok *et al.* [2009] and are applied here in the determination of freeboard. The correction for snow depth biases are taken from Kwok and Cunningham [2008] which relates the albedo dependence of snow depth to the surface reflectivity measured by ICESat. An additional correction to account for remaining residual biases due to contamination of snow and ice within the ICESat footprint is taken from Kwok *et al.* [2009].

[13] The temporal sampling of ICESat is limited to the times shown in Table 2 which restricts our analysis to time periods when ICESat data is available. Throughout we will refer to ICESat campaigns by their campaign name shown in Table 2, the first two letters of the campaign name refer to the months of measurement while the numerals refer to the year (e.g., ON03 for the October–November 2003 campaign). The length of the ON03 campaign made it suitable to split into two subcampaigns for the purposes of comparing the heat flux and ice growth rates between years. The ON03\_1 campaign is at a similar time of year to the ON04 and ON07 campaigns while the ON03\_2 campaign is at a similar time of year to the ON05 and ON06 campaigns. The FM04, FM05, FM06, and FM08 ICESat campaigns occurred during roughly the same time of year while the MA07 campaign occurred later in the ice growth season than all other campaigns.

### 2.4. Sea Ice Thickness and Snow Depth

[14] The sea ice thickness,  $h_i$ , is calculated by assuming local hydrostatic balance and is given by

$$h_i = \frac{\rho_w}{\rho_w - \rho_i} h_f - \frac{\rho_w - \rho_s}{\rho_w - \rho_i} h_s, \quad (1)$$

where  $h_f$  is the height of the snow and ice layers above the water level,  $h_s$  is the snow depth,  $\rho_w = 1024 \text{ kg m}^{-3}$  is the density of sea water,  $\rho_i$  is the density of sea ice taken to be  $915 \text{ kg m}^{-3}$  [Weeks and Lee, 1958; Wadhams *et al.*, 1992], and  $\rho_s$  is the density of snow.  $\rho_s$  is taken to be changing with time following the climatological values compiled by Warren *et al.* [1999], it varies from a minimum of  $260 \text{ kg m}^{-3}$  in early October to a maximum of  $330 \text{ kg m}^{-3}$  at the end of the winter ICESat campaigns.

[15] The large difference between the spatial resolutions of the freeboard (approximately 70 m) and snow depth (25 km) data sets leads to ambiguities when combining these data to estimate sea ice thickness. Due to the nonlinear dependence of the heat flux values on snow and ice thickness (an example of which can be seen in Figure 2 for typical winter time conditions), it is necessary to use a high spatial resolution estimate of the thickness values to properly include the contributions of thin, young ice regions which can be present in any area due to ice dynamics. Kurtz *et al.* [2009] found that the mean heat flux and ice growth values calculated for the Arctic basin using the full 70 m spatial resolution of ICESat were approximately one-third higher than those calculated using 25 km mean thickness values. Therefore, the method developed by Kurtz *et al.* [2009] for combining low-resolution snow depth data with high-resolution freeboard data is used to estimate the snow and ice thickness distributions for each of  $25 \times 25 \text{ km}$  grid cells in the Arctic



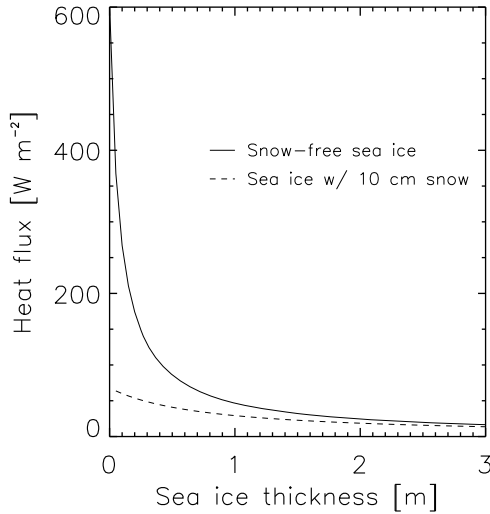


**Figure 2.** Plot of the dependence of the ocean-atmosphere heat flux on sea ice thickness for snow-free and snow-covered sea ice using typical winter time conditions in the Arctic. Input parameters are as follows: air temperature of  $-25^{\circ}\text{C}$ , cloud fraction of 0.5, wind speed of 6 m/s, relative humidity of 0.9, and no shortwave flux.

containing available ICESat freeboard data. The method is based on an observed linear relationship between freeboard and snow depth for thin ice. The linear relationship between freeboard and snow depth applies to points with a freeboard less than a certain cutoff value,  $fb_{cutoff}$ .  $fb_{cutoff}$  is defined as

$$fb_{cutoff} = 0.69\langle h_s \rangle + 0.22\langle h_f \rangle + 5.10,$$

where  $\langle h_s \rangle$  is the mean snow depth of the region which is given by the 25 km resolution snow depth model,  $\langle h_f \rangle$  is the mean freeboard of the ICESat data line within the 25 km snow depth grid cell, and the units of the constant, 5.10, are in cm. A constant snow depth is used for thick ice (where  $h_f > fb_{cutoff}$ ) and is given by

$$hs_{thick} = 1.03\langle h_s \rangle + 0.83,$$

where the units of the constant value, 0.83, are also in cm.  $h_s$  is thus given by

$$h_s = \begin{cases} hs_{thick} \left( \frac{h_f}{fb_{cutoff}} \right) & h_f \leq fb_{cutoff} \\ hs_{thick} & h_f > fb_{cutoff} \end{cases}.$$

Here  $h_f$  is taken from the ICESat data set, and  $h_i$  is then calculated for each freeboard data point using equation 1. The ice thickness distribution for each  $25 \times 25$  km grid cell is then estimated from the approximately 70 m resolution ice thickness data. A minimum of 70 freeboard points (about half the grid cell coverage) are required for the determination of the ice thickness distribution in each grid cell.

### 3. Thermodynamic Sea Ice Model

[16] The ocean-atmosphere heat fluxes and ice growth rates are calculated here through the use of a thermodynamic model with inputs from the data sets described in section 2.

The discrete ICESat ice and snow thickness data points are assumed to represent the thickness distribution in each model grid cell, and the heat flux and ice growth values are calculated for each individual ice thickness data point in a grid cell containing a valid number of measurements. Heat transfer between the ocean, ice, snow, and atmosphere is governed by the temperature of each system, the temperatures of the ocean and atmosphere are specified, while the temperature profiles of the ice and snow are calculated. The temperature of the ocean layer in contact with the ice is taken to be near the freezing point of seawater at  $T_b = 271.35$  K, while the surface air temperature and other relevant meteorological parameters are taken from the ECMWF, AMSR-E, and MODIS data discussed in section 2. Temperature gradients are mainly vertical, therefore disregarding horizontal heat fluxes the temperature distribution within the snow and ice layers is governed by the one-dimensional heat diffusion equations

$$\rho_s c_{snow} \frac{\partial T}{\partial t} = k_s \frac{\partial^2 T}{\partial z^2}, \quad (2)$$

$$\rho_i c_{ice} \frac{\partial T}{\partial t} = k_i \frac{\partial^2 T}{\partial z^2}, \quad (3)$$

where  $c_{snow} = 2.1 \times 10^3$  J kg $^{-1}$  K $^{-1}$  and  $c_{ice} = 2.1 \times 10^3$  J kg $^{-1}$  K $^{-1}$  are the specific heats of ice and snow, and  $k_s = 0.31$  W m $^{-1}$  K $^{-1}$  and  $k_i = 2.04$  W m $^{-1}$  K $^{-1}$  are the thermal conductivities of snow and sea ice, respectively, which are empirical values obtained from *Maykut and Untersteiner* [1969]. A more recent study by *Sturm et al.* [2002] also found the effective thermal conductivity for snow to be approximately 0.3 W m $^{-1}$  K $^{-1}$ . The numerical scheme used to solve equations 2 and 3 follows the three-layer model of *Semtner* [1976] with parameterizations for the individual heat flux terms described in detail below.

[17] The resultant mean surface air temperature, ocean-atmosphere heat flux, and ice growth rates used in sections 4 and 5 are the model average values over each ICESat measurement time period. They were calculated by running the thermodynamic model with 6 h time steps over each specific time period shown in Table 2. The initial temperature profiles of the snow and ice layers were determined by first setting the system in thermodynamic equilibrium then running the model over a one week time period prior to the start of each campaign shown in Table 2.

#### 3.1. Heat Flux Parameterizations

[18] The various heat flux terms are calculated by solving the energy balance equation to find the surface temperature,  $T_0$ , based on the method of *Maykut* [1978]. The energy balance equation at the surface is

$$F_r + F_L - F_E + F_s + F_e + F_c = 0, \quad (4)$$

where  $F_r$  is the net absorbed surface shortwave flux,  $F_L$  the incoming longwave flux,  $F_E$  the emitted longwave flux,  $F_s$  the sensible heat flux,  $F_e$  the latent heat flux, and  $F_c$  the conductive heat flux. A positive flux is defined as being toward the surface while a negative flux is away from the surface.

[19] The net absorbed shortwave flux,  $F_r$ , can be written as

$$F_r = F_{r_0}(1 - \alpha)(1 - i_0), \quad (5)$$

where  $F_{r_0}$  is the shortwave flux reaching the surface,  $\alpha$  is the surface albedo, and  $i_0$  is the percentage of shortwave radiation which passes through the surface and into the water. For snow covered ice  $\alpha$  is 0.8 and  $i_0$  is 0. For ice with a negligible snow cover ( $<1$  cm thick is treated here as snow free)  $\alpha$  is a function of ice thickness,  $h_i$ , and calculated using the empirical relation between ice thickness and albedo described by *Weller* [1972].  $i_0$  is estimated from radiative transfer calculations described by *Maykut* [1982].

[20] Many parameterizations of the  $F_{r_0}$  and  $F_L$  radiative flux terms have been proposed in the literature. *Key et al.* [1996] analyzed various schemes and found that the shortwave parameterization scheme of *Shine* [1984] and the downwelling longwave parameterization scheme of *Maykut and Church* [1973] perform well for Arctic conditions.  $F_{r_0}$  is calculated here following *Parkinson and Washington* [1979] by applying the cloudiness factor of *Laevastu* [1960] to the empirical equation of  $F_{r_0}$  for clear skies described by *Shine* [1984]. The downwelling longwave parameterization scheme of *Maykut and Church* [1973] is used to calculate  $F_L$ .

[21] The emitted longwave radiation,  $F_E$ , is given by

$$F_E = \epsilon \sigma T_0^4, \quad (6)$$

where  $\epsilon$  is the longwave emissivity of the surface layer taken to be 0.99,  $\sigma$  is the Stefan-Boltzmann constant, and  $T_0$  is the temperature of the surface layer.

[22] The turbulent fluxes are calculated using bulk aerodynamic formulas following *Pease* [1987]

$$F_s = \rho c_p C_s u (T_a - T_0), \quad (7)$$

$$F_e = \rho L C_e u (q_a - q_0), \quad (8)$$

where  $\rho$  is the air density,  $c_p = 1004 \text{ J kg}^{-1} \text{ K}^{-1}$  is the specific heat of air at constant pressure,  $C_s = 2 \times 10^{-3}$  and  $C_e = 2 \times 10^{-3}$  are the sensible and latent heat transfer coefficients, respectively, for neutrally stratified air and are adjusted for unstable conditions following *Hack et al.* [1993],  $u$  is the average wind speed,  $L = 2.83 \times 10^6 \text{ J kg}^{-1}$  is the latent heat of sublimation, and  $q$  is the specific humidity. The conductive flux,  $F_c$ , is calculated by following the three-layer model of *Semtner* [1976]. Three vertical grid points are used: one in the snow layer, and two evenly spaced grid points in the ice layer. The surface energy balance equation (equation 4) can now be rewritten through substitution of the parameterizations for  $F_r$ ,  $F_L$ ,  $F_E$ ,  $F_s$ ,  $F_e$ , and  $F_c$ . The surface temperature-dependent terms in the surface energy balance equation are linearized to determine the temperature change of the surface layer for each time step. A time step of 6 h is used to coincide with the temporal resolution of the input ECMWF meteorological data described in section 2. Due to the coarse resolution of the temperature grid, a forward differencing scheme is used to calculate the conductive fluxes across the snow and ice layers and find the temperature profile, which is assumed to be linear between interior grid points. The forward differencing scheme is stable for vertical grid points with  $h_i > 22$  cm and  $h_s > 14$  cm,

so the number of grid points is reduced as needed to maintain computational stability. For the case of ice with a thickness less than 22 cm, the “zero layer” method of *Semtner* [1976] is used to determine the vertical temperature profile, the snow and ice layers are treated as a single system that maintains thermodynamic equilibrium with the external conditions at all times.

[23] The ocean-atmosphere heat flux is defined as the net heat transferred from the ocean to the atmosphere, or  $-F_c$ . For open water areas, the individual heat flux terms are calculated using the above relations for  $F_r$ ,  $F_L$ ,  $F_E$ ,  $F_s$ , and  $F_e$  with suitable changes to  $\alpha$ ,  $i_0$ ,  $T_0$ , and  $L$ . The surface albedo of open water is taken to be 0.08 while  $i_0$  is the amount of shortwave energy passing through the ocean mixed layer which is calculated to be 0.2 based on the results of *Maykut and Perovich* [1987] for a 30 m mixed ocean layer. The latent heat of sublimation,  $L$ , is replaced by the latent heat of vaporization which is  $2.5 \times 10^6 \text{ J kg}^{-1}$ . The surface temperature,  $T_0$ , is replaced by the ocean surface temperature,  $T_w$ .  $T_w$  is taken to be constant at 271.35 K for ice-covered regions. The net ocean-atmosphere heat flux is

$$F_O = F_E - F_r - F_L - F_s - F_e. \quad (9)$$

### 3.2. Thermodynamic Ice Growth Rate

[24] Ablation and accretion of ice at the bottom of the sea ice layer occurs when there is an imbalance between the conductive flux through the bottom of the ice ( $F_{cn}$ ) and the flux of energy from the water to the ice ( $F_O^{\uparrow}$ ). The thermodynamic basal ice growth rate is calculated as

$$\frac{dh_i}{dt} = \frac{1}{Q_i} (F_{cn} - F_O^{\uparrow}), \quad (10)$$

where  $Q_i = 3.02 \times 10^8 \text{ J m}^{-3}$  is the heat of fusion of ice,  $F_O^{\uparrow}$  is estimated to be  $2 \pm 1 \text{ W m}^{-2}$  from the results of *Steele and Boyd* [1998], and  $F_{cn}$  is the conductive flux through the lowest ice grid point. The thermodynamic growth rate is calculated only to estimate the mean rate of ice growth for the observed ICESat thickness distributions, it is not used to change the thickness of the ice with time.

## 4. Results for the Ice-Covered Arctic Ocean

[25] The results presented in this section are for the sea ice covered region of the Arctic Ocean containing valid ICESat data. The ocean-atmosphere heat fluxes and ice growth rates represent approximately a monthly mean value for the study region.

### 4.1. Heat Flux and Ice Growth in Regions Containing ICESat Data

[26] Changes in the percentage distribution of different Arctic sea ice thickness classes over the 2003–2008 time period are shown in Figure 3 for both the fall and winter time periods. A general thinning of the ice cover is observed due to the loss of ice with thickness greater than 3 m. This is consistent with recent studies showing much of the older, thicker multiyear ice cover of the Arctic being replaced with thinner first year ice [*Maslanik et al.*, 2007; *Comiso et al.*, 2008]. Using similar data sets and methods, *Kwok et al.*

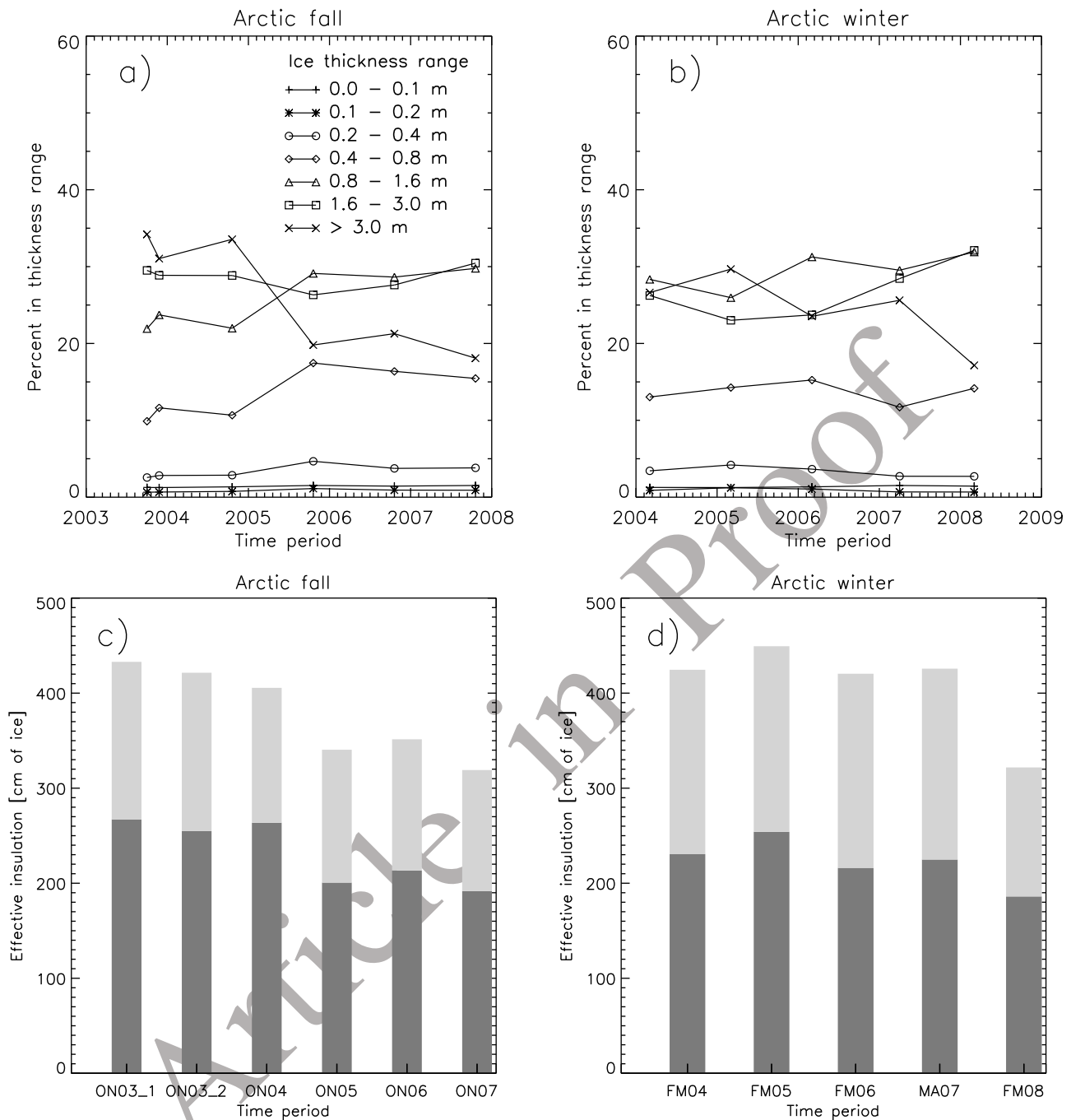


**Figure 3.** Distribution of ice thickness classes over the Arctic basin for the (a) fall and (b) winter ICESat campaigns. (c and d) The mean effective insulation of the snow plus sea ice cover in terms of an equivalent thickness of snow-free sea ice is also shown. The dark colored bars in Figures 3c and 3d represent the sea ice contribution, while the lighter colored bars represent the snow depth contribution.

424 [2009] showed a comparable thinning of the Arctic sea ice  
 425 cover with an overall decrease in the mean thickness over  
 426 the same time period. The sea ice thickness results shown  
 427 here differ from those of *Kwok et al.* [2009] due mainly to  
 428 differences in the sea ice density used (*Kwok et al.* [2009] used  
 429  $\rho_i = 925 \text{ kg m}^{-3}$  while this study uses  $\rho_i = 915 \text{ kg m}^{-3}$ ).  
 430 *Wadhams et al.* [1992] summarize the results of numerous  
 431 field measurements from the 1950s through the 1970s which  
 432 suggest the mean density of sea ice is typically within the

range  $910\text{--}920 \text{ kg m}^{-3}$  for first year ice and  $910\text{--}915 \text{ kg m}^{-3}$  433  
 for multiyear ice. However, whether the density of sea ice has 434  
 changed with time due to changing ice conditions is an 435  
 important, but unknown factor in the determination of sea ice 436  
 thickness. Errors in the calculated heat flux and ice growth 437  
 rates due to uncertainty in sea ice density are discussed in 438  
 section 5. Figure 3 also shows the changes that occurred to 439  
 the mean effective insulation of the sea ice cover over this 440  
 time period. The effective insulation is defined here as the 441

thermal insulating strength of the snow plus sea ice layer in terms of an equivalent thickness of snow-free sea ice, it is calculated as  $h_{\text{eff}} = h_i + \frac{k_i}{k_s} h_s$ . The effective insulation of the fall ice pack decreased significantly in 2005 then remained relatively constant. The loss in the effective insulation during the fall periods is associated mainly with thinning of the sea ice rather than a loss of snow. During the winter time periods, the effective insulation stayed relatively constant until 2008 when it decreased by approximately 1 m (Figure 3). This decrease in the winter of 2008 is due to thinning of both the sea ice and snow covers which is associated with the large loss in multiyear ice and record minimum sea ice extent observed in 2007.

[27] The percentage of ice within a given ice thickness class and the area weighted heat flux values for the various thickness classes are shown in Table 3. Also shown in Table 3 are the following mean input parameters: 2 m air temperature, cloud fraction, wind speed, and the calculated surface temperature. The calculated values are for areas where free-board data from ICESat were available which can be seen in Figures 4 and 5. Areas without ICESat data were not considered in the analysis in this section.

[28] Table 3 shows that over half of the ice production and ocean-atmosphere heat flux ( $-F_c$ ) in the ice-covered regions of the Arctic Ocean occurred over areas with an ice thickness less than 80 cm. In particular, open water and newly refrozen leads with an ice thickness less than 10 cm accounted for nearly one-third of the ocean-atmosphere heat flux and ice production within ice-covered areas. The thickest ice ( $>1.6$  m) is the dominant ice type and was found to make up 50–60% of the total observed ice in the Arctic. Yet, the thickest ice accounted for only 20–30% of the observed ice production and ocean-atmosphere heat flux. The basin wide averaged ice growth rate was generally higher in the winter than in the fall, this was due to the lower surface air temperatures and increased area of first year ice during the winter periods. The percentage contribution of each thickness class to ice production and heat flux varied due to the changing ice thickness distributions and input meteorological parameters. The net radiative flux showed the highest variability of the radiative, turbulent, and conductive heat fluxes. However, if we exclude the anomalous MA07 time period from comparison (which had a higher net radiative flux due to the increased shortwave flux of the later spring period) the net radiation was almost constant and varied by only  $4 \text{ W m}^{-2}$ . The loss of radiative energy by the atmosphere was observed to be much stronger over areas of thick ice rather than thin ice. The sensible heat flux was quite variable with variations of  $8 \text{ W m}^{-2}$  seen during the study period. It acted to transfer heat from the surface to the atmosphere over relatively warm, thin ice ( $h_i < 0.4$  m), while over ice thicker than 0.4 m, it transferred heat from the atmosphere to the surface. Overall, the sensible heat flux was positive owing to the large areas of thick ice in the Arctic, this resulted in a net sensible heat gain by the ice. The latent heat flux varied by  $2 \text{ W m}^{-2}$  for all time periods and was generally a source of small but steady heat input to the atmosphere.

[29] The input forcings and calculated heat flux values from this study are compared with results and observations from studies by Lindsay [1998], Maykut [1982], and Persson *et al.* [2002] in Table 4. The results shown in Table 4 for

this study represent the mean over sea ice 2.75–3.25 m thick to best correspond with the observations conducted on multiyear ice floes in the comparison studies. The computed heat fluxes and forcing parameters derived in this study are within the range of observational values, with the exception of the sensible heat flux and surface air temperature, which were found to be slightly higher during the fall periods. We also compare our results for ice growth rates with those observed during the Surface Heat Budget of the Arctic Ocean (SHEBA) experiment. Perovich *et al.* [2003] studied basal ice growth rates for a 1.75 m thick multiyear ice floe (“Quebec site”) which grew to about 2.25 m thick between early October and March 1998. They report growth rates of  $0.10\text{--}0.30 \text{ cm d}^{-1}$  in the fall and  $0.25\text{--}0.50 \text{ cm d}^{-1}$  in the winter (at comparable times to the fall and winter ICESat campaigns shown in Table 2). For a similar ice thickness class (ice of thickness between 1.75 and 2.25 m), we obtained similar Arctic-wide growth rates of  $0.19\text{--}0.32 \text{ cm d}^{-1}$  (mean  $0.24 \text{ cm d}^{-1}$ ) in the fall and  $0.27\text{--}0.44 \text{ cm d}^{-1}$  (mean  $0.33 \text{ cm d}^{-1}$ ) in the winter. These comparisons demonstrate reasonable agreement between our derived results and observations from previous studies. The major advantage of the remote sensing data sets used here is that it is now possible to calculate the ocean-atmosphere heat flux and ice growth rate for all ice-covered areas of the Arctic. Table 3 thus expands on the knowledge from previous observational studies by providing information over the full range of ice thickness classes of the Arctic Ocean.

[30] Maps of the mean effective insulation, surface air temperature, ocean-atmosphere heat flux, and ice growth rate are shown in Figure 4 for the fall time periods and Figure 5 for the winter time periods. Figures 4 and 5 show that there was great spatial and temporal variability in the effective insulation, air temperature, heat flux, and ice growth rate during the study period. An analysis of the variability in the heat flux and ice growth rate, due to losses in the effective insulation coupled with changes in the meteorological forcings, is the subject of section 4.2.

## 4.2. Analysis of Heat Flux and Ice Growth Variability

[31] The mean values for the ocean-atmosphere heat fluxes and ice growth rates in Table 3 do not show a clear correlation between an increased ocean-atmosphere heat flux/growth rate and the observed decrease in ice thickness and snow depth derived from the ICESat and snow model data sets. This follows since the observed heat flux also depends on the various meteorological forcings with the surface air temperature playing the largest role. Since surface air temperatures in the Arctic tend to be highly variable, it is likely that any trend in the heat flux values over this short 5 year time period is masked by the natural variability caused by variations in the surface air temperature.

[32] The goal of this section is to better understand the causes of the variability that occurred over the study period. That is, we seek to determine whether the observed variability of the heat flux and ice growth is due mainly to changes in meteorological conditions, changes in ice and snow thickness, or uncertainties in the input parameters. First, we first determine the uncertainty in the heat flux and ice growth rates through estimation of the errors in the input parameters. Next we run the thermodynamic model for each time period using constant meteorological forcings to focus



**Table 3.** Thickness Distribution Averages, Ice Production, and Heat Flux Values Over the Ice-Covered Regions of the Arctic Ocean<sup>a</sup>

Thickness Category	ON03_1	ON03_2	FM04	ON04	FM05	ON05	FM06	ON06	MA07	ON07	FM08
<i>Percentage of Ice in Each Thickness Category</i>											
0–0.1 m	1.3	1.3	1.4	1.3	1.7	1.5	1.5	1.4	1.3	1.5	1.3
0.1–0.2 m	0.6	0.7	0.9	0.8	1.2	1.1	1.1	0.9	0.7	0.9	0.7
0.2–0.4 m	2.6	2.8	3.4	2.9	4.2	4.7	3.6	3.7	2.7	3.8	2.7
0.4–0.8 m	9.9	11.6	13.0	10.7	14.3	17.5	15.2	16.4	11.7	15.4	14.2
0.8–1.6 m	21.9	23.7	28.3	22.0	26.0	29.1	31.3	28.6	29.5	29.8	31.9
1.6–3.0 m	29.5	28.9	26.2	28.8	23.0	26.3	23.7	27.6	28.4	30.5	32.1
≥3.0	34.2	31.0	26.6	33.6	29.7	19.8	23.5	21.3	25.6	18.1	17.2
<i>Net Radiation <math>F_r + F_L - F_E</math> (<math>W m^{-2}</math>)</i>											
0–0.1 m	−1.1	−1.3	−1.6	−1.2	−1.6	−1.4	−1.4	−1.4	−0.8	−1.2	−1.4
0.1–0.2 m	−0.3	−0.3	−0.4	−0.3	−0.5	−0.5	−0.5	−0.4	−0.2	−0.4	−0.3
0.2–0.4 m	−0.9	−1.1	−1.3	−1.0	−1.5	−1.8	−1.4	−1.2	−0.7	−1.3	−1.0
0.4–0.8 m	−3.1	−3.9	−4.2	−3.3	−4.6	−5.9	−5.1	−4.8	−2.8	−5.0	−4.8
0.8–1.6 m	−6.1	−6.9	−8.3	−6.3	−7.5	−8.8	−9.1	−7.6	−6.2	−8.8	−9.7
1.6–∞	−14.3	−13.7	−12.8	−14.6	−12.1	−11.3	−10.8	−10.8	−8.7	−12.2	−12.7
Total	−25.8	−27.1	−28.6	−26.7	−27.7	−29.8	−28.2	−26.1	−19.4	−28.9	−29.9
<i>Sensible Heat Flux <math>F_s</math> (<math>W m^{-2}</math>)</i>											
0–0.1 m	−2.7	−3.0	−4.8	−3.0	−4.3	−3.4	−4.1	−3.7	−3.1	−2.5	−3.8
0.1–0.2 m	−0.2	−0.3	−0.5	−0.2	−0.5	−0.3	−0.4	−0.4	−0.2	−0.1	−0.4
0.2–0.4 m	0.0	−0.2	−0.6	−0.2	−0.4	−0.2	−0.2	−0.5	−0.1	0.3	−0.4
0.4–0.8 m	1.0	0.8	0.3	0.8	1.0	1.5	1.7	0.4	0.9	2.2	0.5
0.8–1.6 m	2.9	2.6	3.2	2.6	3.3	3.6	4.5	2.4	3.3	4.7	3.4
1.6–∞	7.0	6.0	6.5	6.9	6.3	5.5	6.0	4.9	5.3	6.8	6.0
Total	7.9	6.0	4.1	6.9	5.3	6.6	7.6	3.2	6.1	11.4	5.3
<i>Latent Heat Flux <math>F_e</math> (<math>W m^{-2}</math>)</i>											
0–0.1 m	−1.0	−0.9	−1.3	−1.0	−1.3	−1.2	−1.3	−1.2	−1.1	−1.0	−1.1
0.1–0.2 m	−0.1	−0.1	−0.1	−0.1	−0.2	−0.1	−0.1	−0.1	−0.1	−0.1	−0.1
0.2–0.4 m	−0.1	−0.1	−0.2	−0.2	−0.3	−0.3	−0.3	−0.3	−0.3	−0.2	−0.2
0.4–0.8 m	−0.2	−0.2	−0.4	−0.3	−0.5	−0.4	−0.6	−0.5	−0.6	−0.2	−0.5
0.8–1.6 m	0.0	0.0	−0.3	−0.1	−0.3	−0.2	−0.4	−0.4	−0.6	0.0	−0.6
1.6–∞	0.6	0.3	0.0	0.4	0.1	0.2	0.0	0.1	−0.2	0.6	−0.2
Total	−0.8	−1.0	−2.4	−1.3	−2.6	−2.0	−2.6	−2.4	−2.8	−0.9	−2.7
<i>Conductive Heat Flux <math>F_c</math> (<math>W m^{-2}</math>)</i>											
0–0.1 m	4.8	5.2	7.6	5.2	7.1	6.0	6.7	6.2	4.9	4.7	6.3
0.1–0.2 m	0.5	0.6	1.0	0.6	1.2	1.0	1.0	0.9	0.5	0.5	0.8
0.2–0.4 m	1.1	1.4	2.1	1.3	2.3	2.2	1.8	1.9	1.1	1.3	1.7
0.4–0.8 m	2.3	3.3	4.3	2.8	4.2	4.9	4.0	4.9	2.4	3.1	4.7
0.8–1.6 m	3.3	4.3	5.5	3.8	4.5	5.4	4.9	5.6	3.6	4.1	6.8
1.6–∞	6.7	7.4	6.3	7.3	5.7	5.6	4.8	5.8	3.6	4.7	7.0
Total	18.7	22.2	26.9	21.0	25.0	25.2	23.2	25.3	16.2	18.4	27.2
<i>Ice Growth Rate (<math>cm month^{-1}</math>)</i>											
0–0.1 m	4.1	4.4	6.5	4.5	6.1	5.1	5.8	5.3	4.2	4.0	5.4
0.1–0.2 m	0.4	0.5	0.9	0.5	1.0	0.8	0.8	0.7	0.4	0.5	0.6
0.2–0.4 m	0.9	1.1	1.8	1.1	1.9	1.8	1.5	1.6	0.9	1.0	1.4
0.4–0.8 m	1.7	2.5	3.5	2.1	3.3	3.8	3.1	3.8	2.0	2.2	3.8
0.8–1.6 m	2.0	2.8	4.2	2.3	3.3	3.8	3.6	4.0	3.1	2.5	5.4
1.6–∞	2.5	3.3	4.6	3.1	3.2	3.1	3.2	3.4	3.8	2.2	5.6
Total	11.6	14.7	21.6	13.6	18.8	18.5	18.0	18.9	14.4	12.5	22.2
<i>Mean Input Parameters</i>											
$\langle T_a \rangle$ (K)	253.8	250.2	244.5	252.9	248.3	251.7	249.1	250.8	253.3	257.8	246.6
$\langle T_s \rangle$ (K)	251.8	248.2	242.7	251.0	246.3	250.2	247.0	249.7	251.8	256.0	245.1
$\langle Cl \rangle$	0.64	0.58	0.42	0.61	0.48	0.58	0.44	0.67	0.55	0.65	0.45
$\langle u \rangle$ ( $m s^{-1}$ )	6.2	5.5	6.2	6.0	6.3	6.2	6.5	6.2	6.8	6.7	5.7

<sup>a</sup>The heat fluxes and ice production rates for the different ice thickness categories have been weighted by the percentage of ice within each respective thickness category.

exclusively on how the observed changes to the sea ice and snow thickness distributions affected the heat flux and growth rates across the Arctic ice pack.

#### 4.2.1. Sensitivity to Input Parameter Uncertainties

[33] We now estimate the sensitivities and uncertainties in the heat flux and growth rate due to variations in the input parameters. To determine the impact of variability in

the input parameters on the heat flux and ice growth rate, the thermodynamic model was run multiple times to simulate variations in each individual parameter separately over a range of values. The goal was to calculate the sensitivities of the heat flux ( $\frac{\partial F_c}{\partial x}$ ) and ice growth rate ( $\frac{\partial g_{growth}}{\partial x}$ ) to the input parameters (x), and estimate an uncertainty value by multiplying the sensitivity by the estimated uncertainty,  $\sigma_x$ . Sea-



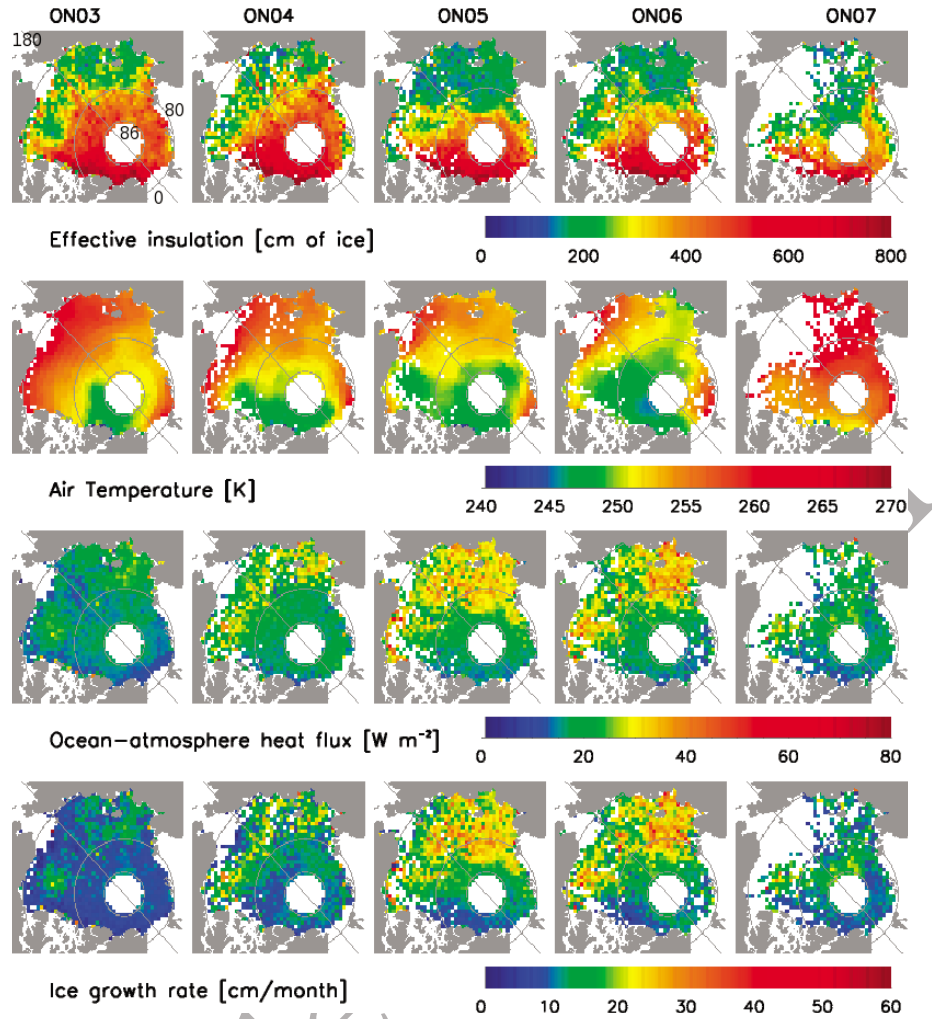


**Figure 4.** Map of the effective insulation, snow depth, and air temperature parameters and the calculated ocean-atmosphere heat fluxes and ice growth rates for the fall measurement periods.

578 sonal sensitivities were calculated and used in the estimation  
 579 of the uncertainties of the heat fluxes and ice growth rates in  
 580 section 4.2.2. Average values of the calculated sensitivities  
 581 and estimated uncertainties for the fall and winter time  
 582 periods are shown in Table 5. In the following discussion,  
 583 only the freeboard uncertainties are assumed to be from a  
 584 zero mean random process. All other error sources are not  
 585 well constrained, thus the net error estimates  $\sigma_{F_e}$  and  $\sigma_{growth}$   
 586 presented in Table 5 are RSS errors calculated from the  
 587 individual error terms.

588 [34] Estimating uncertainties for the meteorological input  
 589 parameters is challenging since errors in the ECMWF Interim  
 590 surface air temperature, and wind speed for the Arctic have  
 591 not been adequately determined at this time. For sea ice  
 592 covered regions, the ECMWF meteorological parameters are  
 593 modeled assuming a uniform snow-free 1.5 m thick ice slab,  
 594 ice concentration is considered using a blend of model and  
 595 observation data [Stark *et al.*, 2007]. As shown in Figures 4  
 596 and 5, the assumption of a uniform effective ice thickness  
 597 of 1.5 m is typically not valid which may impact the ECMWF  
 598 model results. The uncertainties in the ECMWF data depend  
 599 not only on the model accuracy, but also on the quantity and

quality of observations used in the assimilation which can  
 vary considerably in time and space. Here we estimate the  
 uncertainties in these values by assuming that they represent  
 50% of the maximum observed variability of the areal mean  
 across similar time periods. For example, the mean surface  
 air temperature of the ice-covered Arctic,  $\langle T_a \rangle$ , varied from  
 253.3–257.9 K between the ON03\_1, ON04, and ON07  
 campaigns leading to an observed variability of 4.6 K and  
 an estimated uncertainty of 2.3 K. Similarly, uncertainties of  
 0.6 m/s were estimated for the wind speed. Lupkes *et al.*  
 [2010] compared ECMWF Interim near surface air tem-  
 peratures and wind speeds to data from several ship cruises  
 in the late summer in the Arctic and found a warm bias of  
 1.5–2 K in the Interim temperature data set and near zero  
 error in the wind speed. While this bias in the summer data  
 may not apply to the fall and winter time periods used in  
 this study, it suggests that our uncertainties for the surface  
 air temperature and wind speed may be a reasonable estimate.  
 However, the uncertainty in the surface air temperature may  
 vary regionally as it depends on the number of observations  
 used in the assimilation. Additionally, the low resolution of  
 the ECMWF data could potentially lead to errors near the ice

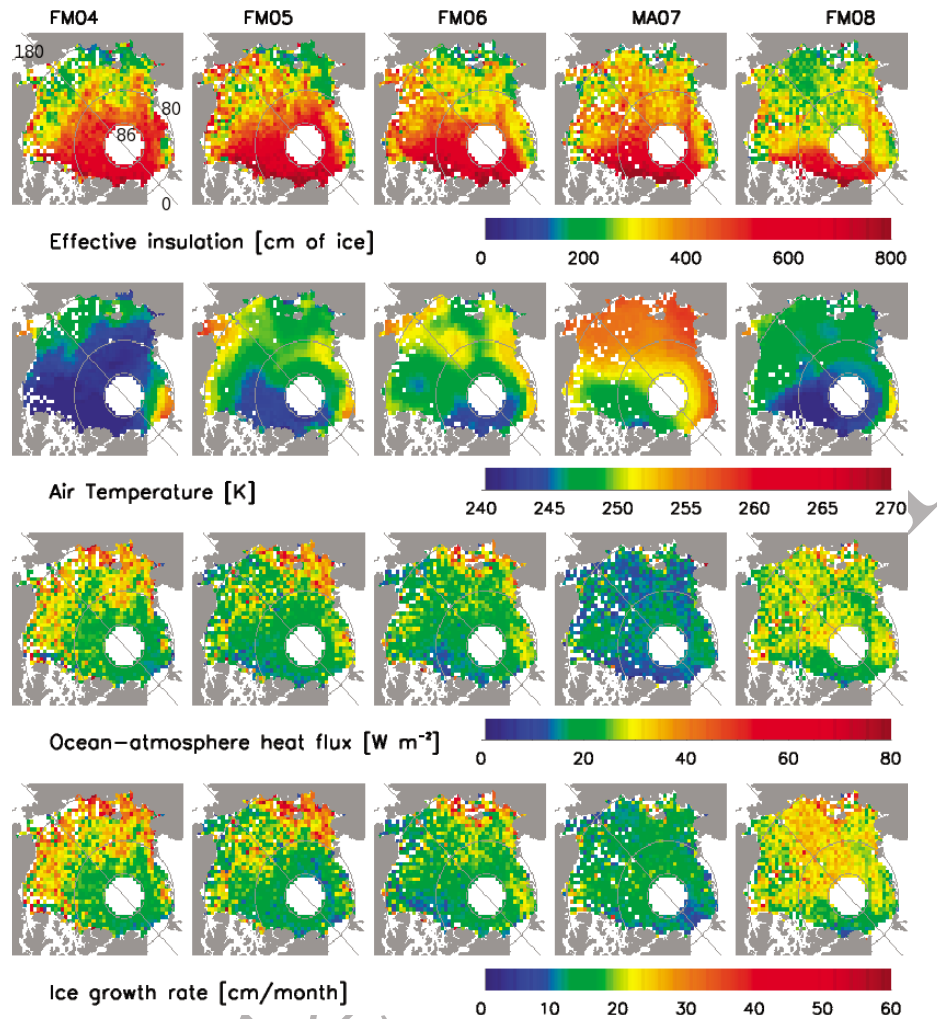


**Figure 5.** Map of the effective insulation, snow depth, and air temperature parameters and the calculated ocean-atmosphere heat fluxes and ice growth rates for the winter and early spring measurement periods.

edge. Errors in the MODIS cloud fractions are estimated to be 0.1 for the Arctic region based on a study by Ackerman *et al.* [2008].

[35] Errors in the ice thickness and snow depth input parameters are due to uncertainties in the freeboard, snow depth, and density values. Errors in the freeboard were

assumed to be unbiased (after the corrections for biases due to snow and ice contamination were applied) but estimated to have a random normally distributed error of  $\sigma_{fb_{si}} = 5$  cm [Kwok and Cunningham, 2008].  $\sigma_{\rho_i}$  is estimated to be 10 kg/m<sup>3</sup> which represents the range of expected densities for sea ice between 0.3 and 3 m thick [Kovacs, 1996].  $\sigma_{\rho_s}$  is

**Table 4.** Comparison of Heat Flux and Forcing Parameters for the Mean of All 2.75–3.25 m Thick Ice Areas With Observations<sup>a</sup>

Parameter	This Study (2.75–3.25 m Ice Only)	L98	M82	P02
Net radiation	−22 (−23)	−24 (−26)	−23 (−18)	−20 (−20)
$F_s$	12 (11)	8 (4)	12 (5)	5 (5)
$F_e$	0 (1)	1 (0)	0 (−2)	−1 (1)
$F_c$	11 (11)	—	11 (14)	6 (10)
$T_a$ (K)	248 (252)	241 (250)	242 (249)	251 (250)
$u$ (m s <sup>−1</sup> )	6 (6)	4 (4)	5 (5)	5 (7)
CI	0.5 (0.6)	0.5 (0.6)	—	—

<sup>a</sup>Observations are from Lindsay [1998] (L98), Maykut [1982] (M82), and Persson *et al.* [2002] (P02). Values from M82 are taken from the 3 m ice thickness results. Values for the fall time periods are in parentheses, while those for the winter are not.

**Table 5.** Sensitivity of the Ocean-Atmosphere Heat Flux and Ice Growth Rate to Variations in the Input Parameters<sup>a</sup>

x	$\sigma_x$	Heat Flux (W m <sup>−2</sup> )		Growth Rate (cm month <sup>−1</sup> )	
		$\frac{\partial F_e}{\partial x}$	$\sigma_x \frac{\partial F_e}{\partial x}$	$\frac{\partial \text{growth}}{\partial x}$	$\sigma_x \frac{\partial \text{growth}}{\partial x}$
$T_a$ (K)	2.3	1.1(1.0)	2.5(2.3)	0.9(0.8)	2.1(1.8)
CI (%)	10	0.02(0.01)	0.2(0.1)	0.02(0.01)	0.2(0.1)
$u$ (m s <sup>−1</sup> )	0.6	0.8(0.8)	0.5(0.5)	0.7(0.7)	0.4(0.4)
$fb_{si}$ (cm)	5	0.3(0.3)	1.6(1.5)	0.3(0.3)	1.4(1.3)
$h_s$ (cm)	5	0.02(0.01)	0.09(0.04)	0.02(0.01)	0.08(0.04)
$\rho_i$ (kg m <sup>−3</sup> )	10	0.1(0.1)	0.9(0.8)	0.1(0.1)	0.8(0.7)
$\rho_s$ (kg m <sup>−3</sup> )	100	0.01(0.01)	0.7(1.2)	0.01(0.01)	0.6(1.0)
$F_0$ (W m <sup>−2</sup> )	1	—	—	0.9	0.9(0.9)
$\sigma_{F_e}$	—	—	3.3(3.2)	—	—
$\sigma_{\text{growth}}$	—	—	—	—	2.8(2.7)

<sup>a</sup>Results for the winter time periods are in parentheses.

634 estimated to be  $100 \text{ kg/m}^3$  based on the variability of  $\rho_s$  in  
 635 the climatology of *Warren et al.* [1999]. Uncertainties and  
 636 sensitivities due to variations in the density of sea water,  
 637 dew point temperature (humidity), and surface air pressure  
 638 are small and not considered here. Errors in the snow depth  
 639 are unknown and estimated to be 5 cm here, but this value  
 640 will be shown to be of small importance in the following  
 641 discussion.

642 [36] Table 5 shows that most of the uncertainty in both the  
 643 heat flux and ice growth values is due to the relatively large  
 644 uncertainty estimated for  $T_a$  with lesser contributions due to  
 645 uncertainty associated with sea ice freeboard, cloud fraction,  
 646 wind speed, snow density, and ice density. Errors due to  
 647 snow depth uncertainties are minor and contribute little to  
 648 uncertainties in the heat flux and growth rates since errors in  
 649 the snow depth are nearly canceled by the corresponding  
 650 retrieval errors in ice thickness. Essentially, 1 cm of snow has  
 651 an effective insulation of  $k_i/k_s = 6.5 \text{ cm}$  of ice, while a 1 cm  
 652 error in snow depth leads to a corresponding error of  $\frac{\rho_w - \rho_s}{\rho_w - \rho_s} \approx$   
 653 6.5 cm in ice thickness which makes errors due to snow depth  
 654 uncertainties small. In this assessment, errors in the calculated  
 655 mean heat flux and ice growth rate values for the Arctic are  
 656 primarily due to errors in  $T_a$ . However, changes in the cloud  
 657 cover and associated incoming longwave radiation can also  
 658 lead to changes in the surface air temperature which cannot  
 659 be studied with a simple model such as the one used here.  
 660 Aside from the impacts to surface air temperature, cloud  
 661 cover changes are not a strong source of variability in the  
 662 sensitivity of the ice growth rate and heat flux values. To  
 663 better estimate the errors in the heat fluxes and ice growth  
 664 rates calculated here, additional studies of the error in the  
 665 ECMWF data for  $T_a$  in the Arctic during the fall and winter  
 666 time periods are needed. The next largest source of error is  
 667 due to freeboard uncertainties, these errors are due to instru-  
 668 mental uncertainties and set a lower limit for the total  
 669 uncertainty in the calculated heat flux and ice growth rate.

#### 670 4.2.2. Heat Flux Variability in Ice-Covered Regions

671 [37] The sensitivity results for the various meteorological  
 672 forcings shown in Table 5 demonstrate that changes in  $T_a$   
 673 are much more dominant than  $Cl$  and  $u$  in affecting vari-  
 674 ability in the calculated heat fluxes and ice growth rates.  
 675 Variability in the surface air temperature is therefore one of  
 676 the main factors that must be considered in analyzing the  
 677 observed variability in the ocean-atmosphere heat flux and  
 678 ice growth rate. Figure 6 shows the mean ocean-atmosphere  
 679 heat flux and ice growth rate for the ice-covered Arctic  
 680 Ocean over the different time periods as well as the corre-  
 681 sponding mean surface air temperatures. The observed heat  
 682 fluxes and growth rate values can be seen to primarily change  
 683 with variations in the surface air temperature. However, the  
 684 changes in the ON05, ON06, ON07, and FM08 time periods  
 685 are disproportionate compared to earlier changes in  $T_a$ . The  
 686 ON05 and ON06 heat fluxes were much higher than those  
 687 observed during the ON03\_2 time period despite the higher  
 688 surface air temperatures. Similarly, the winter FM08 time  
 689 period has a higher heat flux than the FM04 time period  
 690 despite a higher surface air temperature of 2.1 K. Figure 3  
 691 shows that there was a significant change in ice thickness  
 692 distribution and an associated large decline in the effective  
 693 insulation during these time periods. The percentage of ice  
 694 with a thickness greater than 3 m experienced the greatest  
 695 decline beginning around the fall of 2005 and this was

696 accompanied by an increase in the percentage of 0.4–1.6 m  
 697 ice in the fall and 0.8–1.6 m ice in the winter. As shown in  
 698 Figure 2, the ocean-atmosphere heat flux is sensitive to  
 699 changes in the percentage of thin ice, especially for ice less  
 700 than approximately 1 m thick. The percentage of the thin-  
 701 nest ice classes ( $<0.4 \text{ m}$ ) did not change significantly over  
 702 the 2003–2008 time period, however this value is reported  
 703 for the ice-covered Arctic only and does not take into  
 704 account the large changes in open water and loss of ice area  
 705 for the entire Arctic also observed during this time period.

706 [38] The FM05 and FM06 time periods have similar mean  
 707 growth rates, heat fluxes, and surface air temperatures  
 708 (Figures 6b and 6d) even though there was a decline in the  
 709 percentage of thick ice during this time and a decline in  
 710 mean ice thickness of 38 cm. The decrease in the percentage  
 711 of the ice  $>3 \text{ m}$  thick was compensated by an increase in the  
 712 percentage of ice 1.6–3.0 m thick (Figure 3b). Since the  
 713 ocean-atmosphere heat flux and ice growth are much less  
 714 sensitive to changes for ice in this thickness range it appears  
 715 that variability in heat flux and ice growth during these  
 716 winter time periods was dominated more by variability in  
 717 the surface air temperature. The MA07 heat flux and growth  
 718 rate is much lower than the other winter time periods, this is  
 719 likely due to the higher surface air temperatures resulting  
 720 from the later date of data collection as well as thicker ice  
 721 cover due to the longer time available for sea ice growth.

722 [39] The full effect of the observed increase in the ocean-  
 723 atmosphere heat flux due to a thinning of the ice and snow  
 724 cover is difficult to quantify since the ocean-atmosphere heat  
 725 flux and surface air temperature are coupled. The ocean-  
 726 atmosphere heat flux will increase with decreasing tempera-  
 727 ture and vice versa until an equilibrium is reached between  
 728 the surface heat flux and other factors (such as atmospheric  
 729 energy transport) which determine the surface air tempera-  
 730 ture. Nevertheless, to investigate the effect of changes in the  
 731 snow and ice thickness distribution on the observed heat  
 732 flux values (independent of changes due to meteorological  
 733 conditions), we ran the thermodynamic model for the ice  
 734 and snow thickness distributions for each individual time  
 735 period using the same fixed meteorological conditions.  
 736 Figure 7 shows the ocean-atmosphere heat flux differences  
 737 for the individual time periods under the same meteorological  
 738 conditions relative to the first campaign of the fall or winter  
 739 season. This shows that thinning of the sea ice and snow  
 740 covers led to potential ocean-atmosphere heat flux increases  
 741 of nearly  $6 \text{ W m}^{-2}$  for the fall 2005–2007 time periods  
 742 compared to the 2003 time period (an increase of approxi-  
 743 mately 40% over the heat flux observed in ON03\_1). Despite  
 744 the similarly large decrease in the effective insulation  
 745 observed in ON05 and FM08 (Figure 3), the FM08 ocean-  
 746 atmosphere heat flux would only be  $2 \text{ W m}^{-2}$  higher than  
 747 FM04 under equivalent meteorological conditions (an increase  
 748 of approximately 10% from the observed heat flux in FM08),  
 749 but this is also within the uncertainty of the values.

750 [40] The results show that the observed thinning of sea ice  
 751 during the 2005–2008 time period led to large increases in  
 752 the ocean-atmosphere heat fluxes for the subsequent fall  
 753 periods. The increased ocean-atmosphere heat flux likely  
 754 impacted the surface air temperatures and may have played  
 755 a part in the surface air temperature anomalies observed  
 756 during this same period by *Serreze et al.* [2009]. The winter  
 757 results suggest that despite losses in ice thickness and

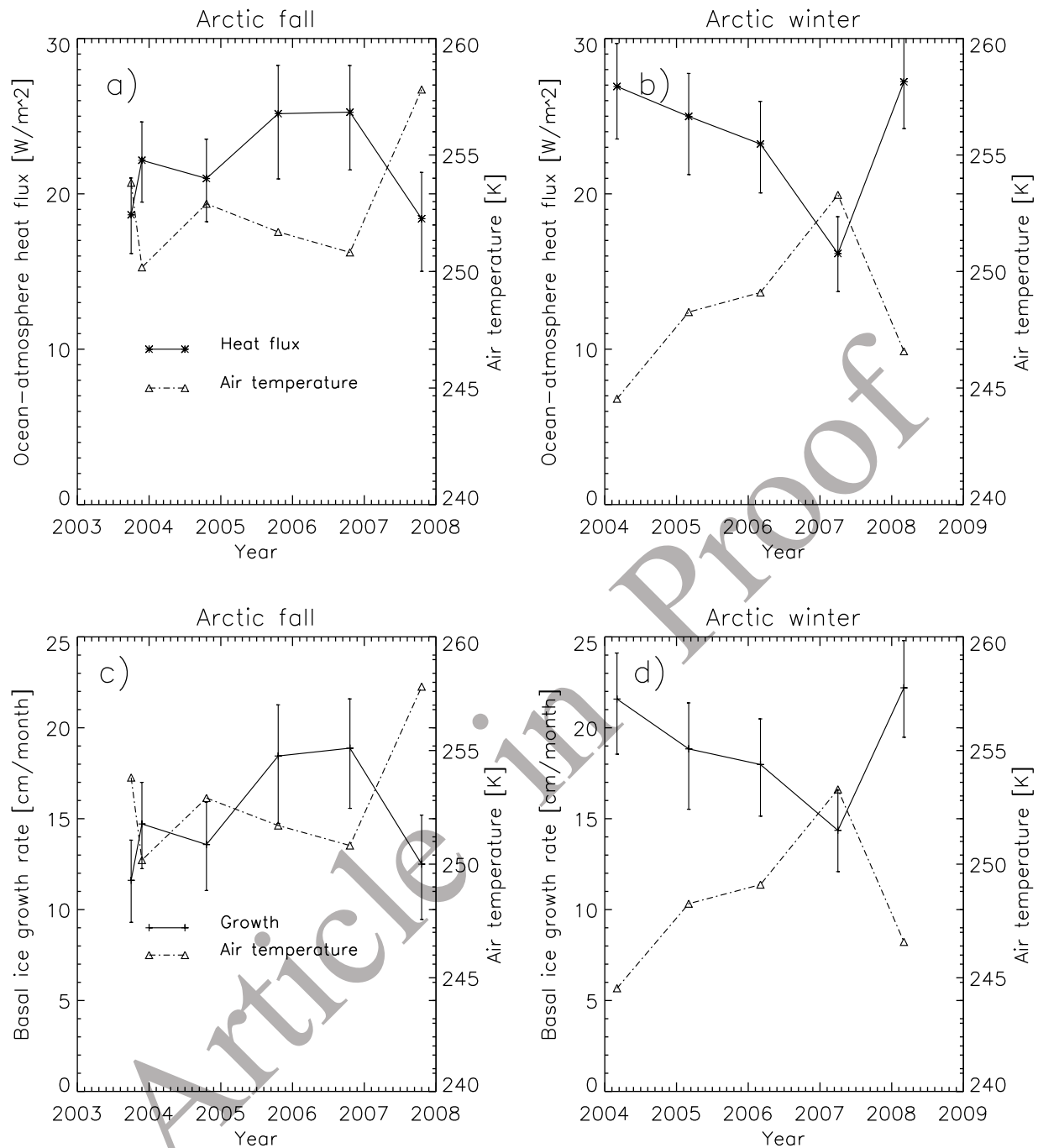


**Figure 6.** The mean ocean-atmosphere heat flux, basal ice growth rate, and 2 m air temperature for ice-covered regions during the Arctic fall and winter seasons.

758 effective insulation, growth of the sea ice and the addition of  
 759 snow over the fall and early winter limited increases to the  
 760 winter heat flux. The MA07 results show a lower equivalent  
 761 heat flux than FM04 which is due to the additional time for  
 762 growth for the thin ice classes which reduces the overall  
 763 heat flux. The FM08 results suggest that an increase in the  
 764 ocean-atmosphere heat flux may be beginning to appear in  
 765 the winter due to the large decrease in ice and snow thickness  
 766 (effective insulation), however this cannot be fully deter-  
 767 mined here due to uncertainties in the input parameters.

#### 4.3. East and West Arctic Differences

[41] Sections 4.1 and 4.2.2 showed that ice thickness and  
 energy exchange for the ice-covered regions of the Arctic  
 Ocean experienced changes for the 2003–2008 time period,  
 however certain regions of the Arctic were impacted dif-  
 ferently than others. Here we discuss the regional impact of  
 such changes by dividing the Arctic into two regions, East  
 Arctic ( $0^\circ$ – $180^\circ$  longitude) and West Arctic ( $180^\circ$ – $360^\circ$   
 longitude), for the purpose of studying the regional vari-  
 ability of ice thickness, energy exchange, and ice growth.



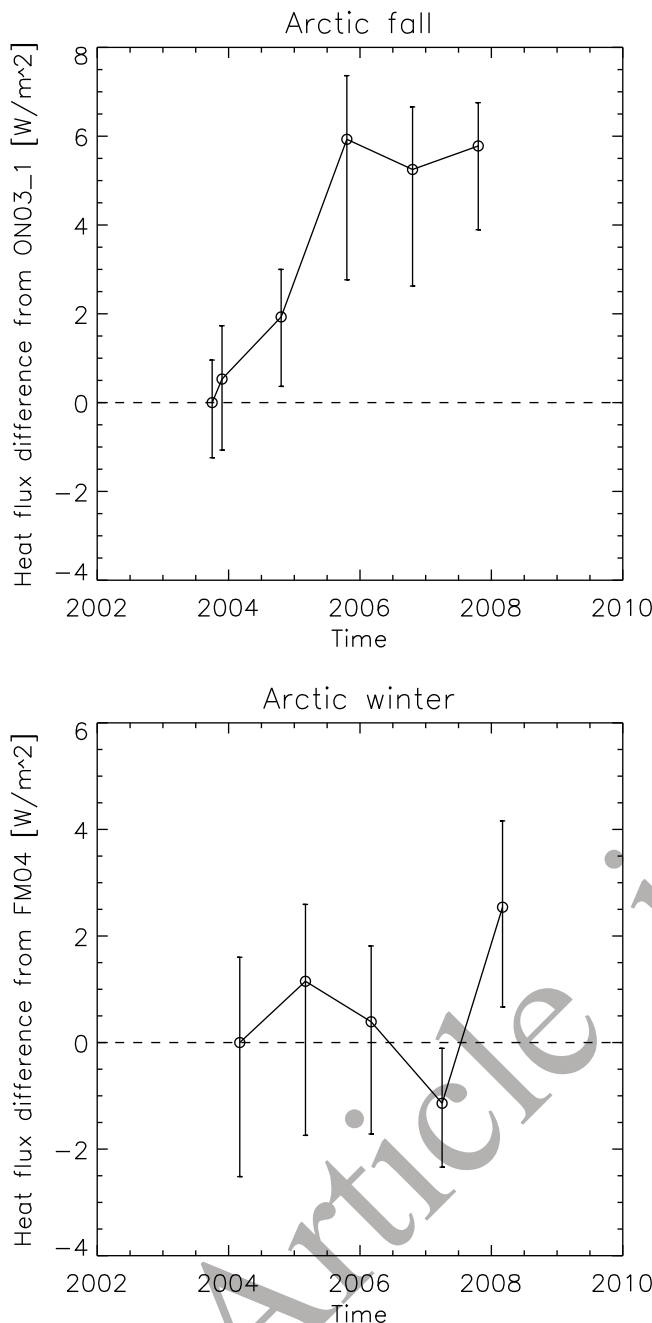


**Figure 7.** Ocean-atmosphere heat flux differences for the different time periods under the same meteorological conditions, differences are relative to the first campaign of the season. The error bars for the heat flux differences are taken from the combined uncertainties from the freeboard, snow depth, snow density, and ice density uncertainties discussed in section 4.2.1.

The regional ice thickness distributions, mean surface air temperatures, and mean growth rates are discussed. The mean growth rate and heat flux terms are used interchangeably here since the two are closely related.

[42] Figure 8 shows a large decline in the amount of thick ice (>3 m) in both regions during the fall periods, with the East Arctic showing a particularly steep decline in 2005.

Much of the ice of thickness greater than 3 m was replaced by ice 0.4–1.6 m thick, with large increases in the 0.2–0.8 m ice thickness class in the East Arctic. Both regions experienced similar variabilities in the surface air temperature, but differences in growth rate variabilities can be seen between the eastern and western Arctic regions due to differences in the ice thickness distribution. In 2005 and 2006 the East Arctic region experienced sharp increases in the ice growth rate/heat flux compared to the ON03\_1 period (which had a lower surface air temperature) due largely to the increased amount of 0.2–0.8 m thick ice. The West Arctic region experienced similar, but less prominent, increases in the ice growth/heat flux in 2005 and 2006 due to the loss of thick ice >3 m.

[43] Figure 9 shows the regional thickness distributions, ice growth rate, and surface air temperature for the winter periods. The East Arctic winter time periods also experienced a general decline in the percentage of thick ice >3 m while the West Arctic did not see large changes in the ice thickness distribution until 2008. Despite losses in the thickest ice category as well as the overall mean ice thickness, the ice growth rate/heat flux is similar for the respective regions with similar surface air temperatures. Thus, as was observed in section 4.2 for the ice-covered Arctic, most of the winter time variability in ice growth rates appears to be due to changes in surface air temperature rather than due to changes in the ice thickness distribution.

## 5. Results for the Full Arctic Ocean

[44] Section 4 showed changes to the ocean-atmosphere heat flux and ice growth rate for areas containing ICESat data. We now extend the analysis to the full Arctic Ocean, including open water areas, to better place the results into context given the large changes in sea ice areal coverage over the time period.

[45] In this section, the heat flux and ice growth rates are calculated for nonice-covered areas by using sea surface temperature data described in section 2. Areas with an ice concentration greater than 0 and less than 30% were treated initially as open water, but with a sea surface temperature at the freezing point of sea water. For the nonice-covered areas, the ice growth rate and ocean-atmosphere heat flux were calculated at 6 h time intervals. If the sea surface temperature was at the freezing point the ice was allowed to grow in thickness and the growth rate was approximated from the net surface heat flux and equation 10, if the sea surface temperature was greater than freezing point of sea water then the ice thickness and growth rates were set to 0. Without the insulation of a sea ice cover, the net surface heat flux tended to be much larger than that from the ice-covered regions. However, the rate of ice growth rate is not directly proportional to the net surface heat flux in nonice-covered areas because of the limitation that ice will only grow once the surface temperature has reached the freezing point.

[46] To determine the net heat output and ice production of the Arctic Ocean, we first grid the heat flux and ice growth rate data onto a 25 km polar stereographic grid. Gaps in the gridded data were filled in through the use of a Gaussian smoother with a 20 km length scale (following Kwok *et al.* [2009]). Ice-covered and nonice-covered areas were filled in independently using their respective data sets. The pole

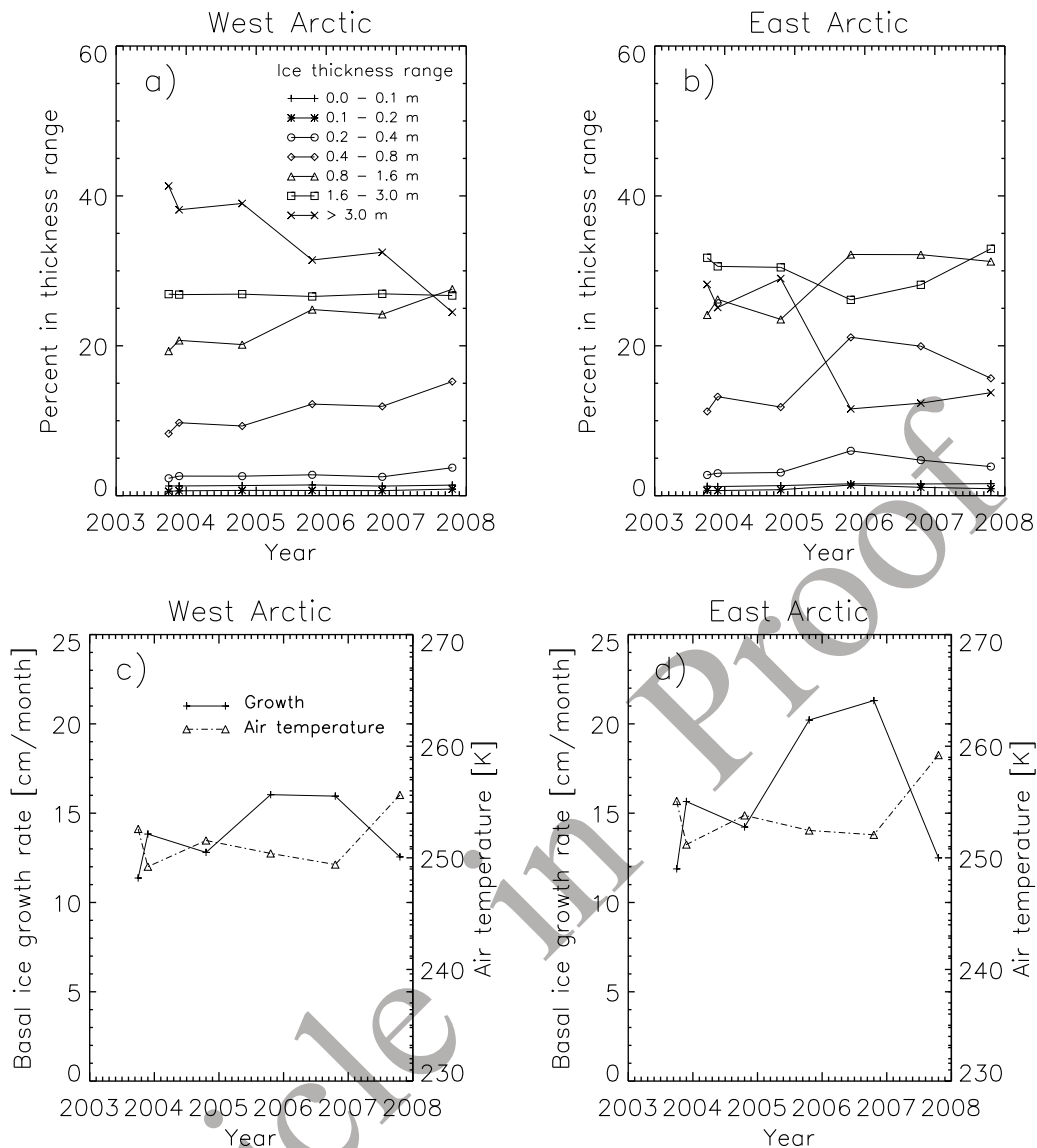


**Figure 8.** Fall time period ice thickness distributions, mean basal ice growth rates, and mean surface air temperatures for the ice-covered east and west Arctic regions.

845 hole north of 86 degrees was not filled in due to the large  
846 uncertainty introduced in interpolating the data over such a  
847 large region. The total area of the Arctic Ocean considered  
848 in this section for all time periods is  $6.47 \times 10^6 \text{ km}^2$ . The  
849 net surface heating rate and net ice volume production are  
850 this area value multiplied by the ocean-atmosphere heat flux  
851 and ice growth rates, respectively. Results for the net surface  
852 heating rate and ice volume production as well as the areal  
853 coverage of ice and nonice areas are shown in Figure 10.

#### 854 5.1. Net Arctic Ocean Heat Output

855 [47] Figure 10c shows an increasing trend in the total  
856 Arctic Ocean heating rate for the fall periods, while  
857 Figure 10d shows comparatively little change in the winter  
858 heating rate. Figures 10a and 10d show that for sea ice-  
859 covered regions, the net heating rate did not change mark-  
860 edly compared to the full Arctic Ocean domain in both the  
861 fall and winter. The heating rate over nonice-covered areas

changed most dramatically in 2007 due to the larger amount  
of open water in that year (Figures 10b and 10e), increasing  
by nearly a factor of 5 from the previous years. Though ice-  
covered areas made up the dominant portion of the Arctic  
Ocean, the total heating rates were nearly equal over ice-  
covered and nonice-covered areas for the fall periods (with  
the exception of 2007). In 2004, 2005, and 2006 the net  
heating rate increased by 44%, 17%, and 12% from 2003,  
respectively. While in 2007 the large increase in nonice-  
covered areal coverage caused the total heating rate for the  
Arctic Ocean to increase by 300% from that in 2003. With  
the exception of the much later MA07 measurement time  
period, there was much less change in the winter time  
heating rates with a maximum change of 16% observed.

[48] The results show an overall increase in the amount  
of ocean-atmosphere heat transfer in the fall periods.  
Section 4.2.2 showed that independent of changes in mete-  
orological conditions, thinning of the sea ice cover is

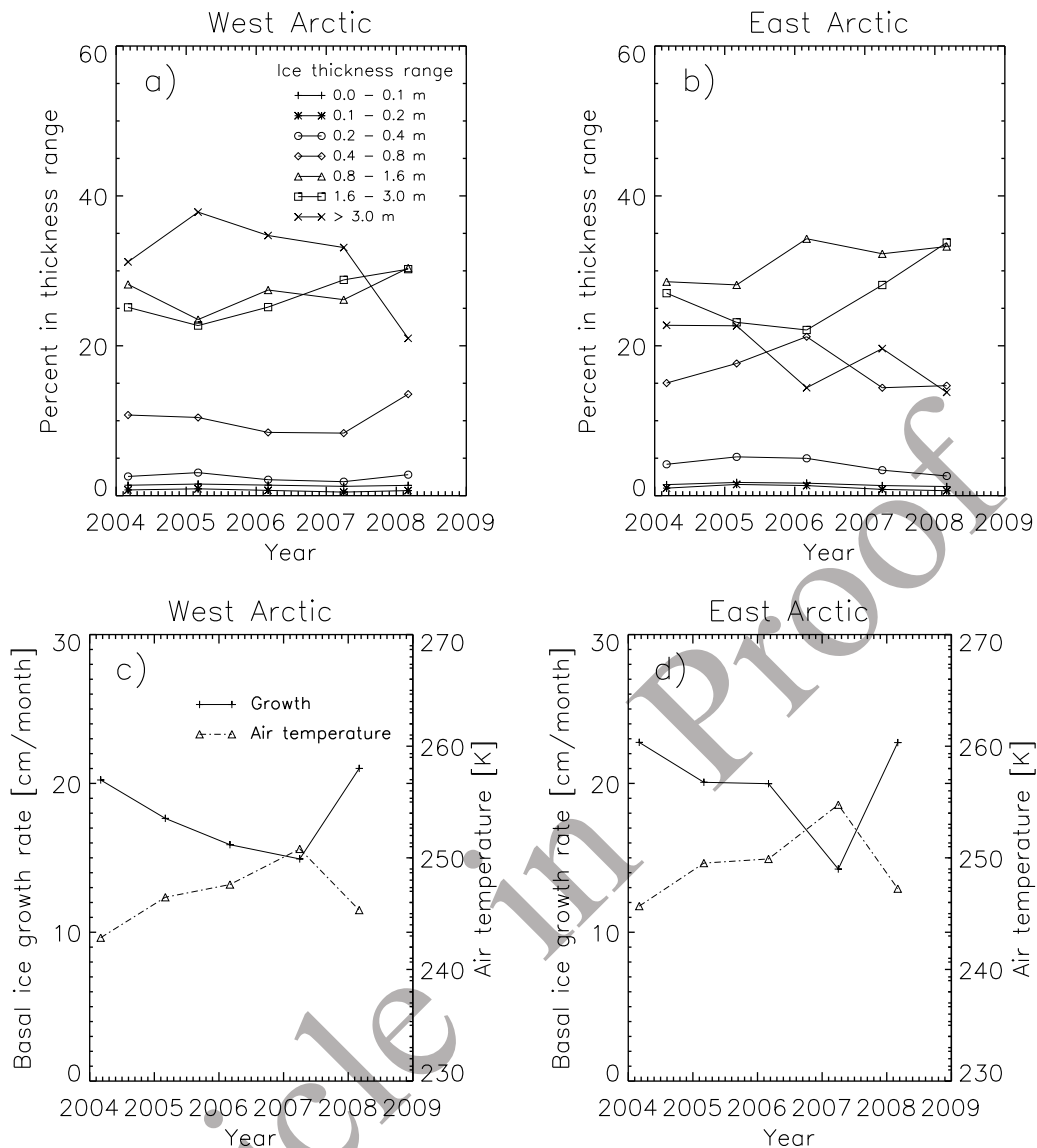


**Figure 9.** Winter time period ice thickness distributions, mean basal ice growth rates, and mean surface air temperatures for the ice-covered east and west Arctic regions.

responsible for up to a 40% increase in the net heat output in the ice-covered Arctic Ocean. However, this increase is small compared to the effect caused by changes in the ice areal coverage. The anomalously low areal coverage of sea ice in 2007 marked a turning point where the net Arctic Ocean heating rate became dominantly determined by the amount of ice-free area.

## 5.2. Net Arctic Ocean Ice Production

[49] The observed changes in sea ice thickness and ocean-atmosphere heat flux also lead to changes in the ice growth rate. Of particular interest is whether the observed losses in sea ice thickness and areal coverage led to a higher rate of ice production which could aid in the recovery of sea ice thickness and volume.

[50] For sea ice-covered regions, the mean basal ice growth rates are shown in Table 6. Though basal ice growth varied with time depending on the surface air temperature

and ice thickness distribution in a similar manner as the heat flux, Table 6 shows that a higher growth rate in the fall was generally followed by a lower growth rate in the winter and vice versa. The observed decreases in ice thickness may be due to a longer melt season as observed by Markus *et al.* [2009], increased oceanic heat flux as observed for the western Arctic by Woodgate *et al.* [2010], and/or increased ice export rather than due to changes in ice growth. These observations show that an expected increased basal ice growth rate associated with decreasing ice thickness did not largely occur over the 2003–2008 time period mainly due to associated changes in the surface air temperature.

[51] The rate of ice volume production for ice-covered and nonice-covered areas is shown in Figure 10, the production of ice can be seen to vary considerably from year to year. For the fall season ice-covered portion of the Arctic Ocean, the production of ice peaked in 2005 and 2006 due in part to the thinning of the ice cover and associated

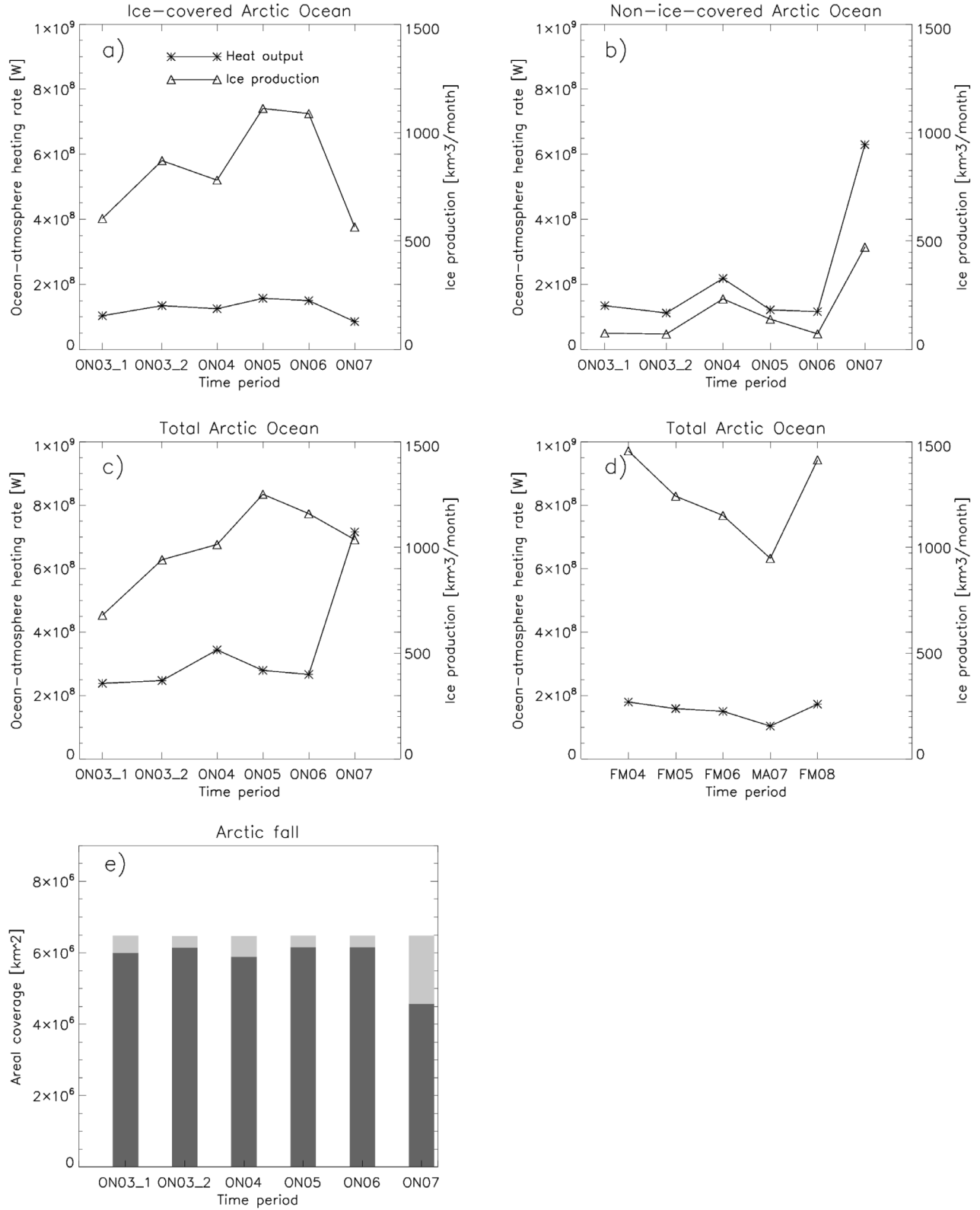


**Figure 10.** Net ocean-atmosphere heating rate and ice volume production for the (a) ice-covered, (b) nonice-covered, and (c and d) total Arctic Ocean. (e) The dark colored bars represent the areal coverage of ice-covered regions, and the light colored bars represent the nonice-covered areal coverage. For the winter time periods, all regions are ice covered. The total area of the Arctic Ocean domain for all time periods in this study is  $6.47 \times 10^6 \text{ km}^2$ .



Table 6. Basal Ice Growth Rate for Ice-Covered Regions During the Fall and Winter Seasons<sup>a</sup>

	2003–2004	2004–2005	2005–2006	2006–2007	2007–2008
Fall ice growth (cm month <sup>-1</sup> )	10.1 (14.2)	13.3	18.1	17.7	12.4
Winter ice growth (cm month <sup>-1</sup> )	22.6	19.2	17.8	14.7	21.9

<sup>a</sup>The ON03\_2 period is shown in parentheses.

increased ocean-atmosphere heat flux discussed in section 4. In 2007, the production of ice in ice-covered regions reached the lowest point due to the high surface air temperatures and low ice areal coverage of the time period, while in nonice-covered areas the ice production increased by nearly a factor of 3 compared to the previous fall seasons. [52] For the full Arctic Ocean fall periods, the combination of ice production in ice-covered and nonice-covered areas led to a peak in the ice production in 2005 and a decrease in the following years. Despite the large increase in total ocean-atmosphere heat output in 2007, warm ocean and air temperatures kept the level of ice production near to that of 2004. Thus, the 2007 ice minimum led to a greatly increased release of heat from the ocean to the atmosphere, however this increased heating rate did not lead to an increase in overall ice production because the ocean had yet to cool to the freezing point. The winter period ice production was much less variable, excluding the much later MA07 measurement period the ice production varied by less than 20% over the 2004–2008 time period. The winter time ice production variability was driven primarily by variability in the surface air temperature.

## 6. Summary and Discussion

[53] In this study we have combined ICESat freeboard retrievals with a snow depth model to estimate snow and sea ice thickness values for the Arctic Ocean during the 2003–2008 fall and winter time periods. The thickness data were used with meteorological data and a thermodynamic sea ice model to calculate the turbulent, radiative, and conductive heat fluxes, as well as the total ocean-atmosphere heat output and ice volume production for the Arctic Ocean. Sensitivities to the input parameters were determined and used to estimate the error in the calculated ocean-atmosphere heat fluxes and ice growth rates. The main factor affecting the uncertainty in our results was found to be uncertainties in the surface air temperature. Laser altimetry data was found to be particularly useful for determining the heat fluxes since the results are relatively insensitive to snow depth errors.

[54] The heat flux and ice growth rates in ice-covered regions presented here are consistent with those from previous observational studies conducted on multiyear ice. The advantage of the data sets used in this study is that they allow for estimates of heat flux over the entire Arctic basin. Also in agreement with the results of previous studies [e.g., Kwok *et al.*, 2009; Giles *et al.*, 2008; Maslanik *et al.*, 2007], this study shows that during the 2003–2008 time period the mean Arctic sea ice thickness decreased with much of the thickest ice (>3 m) being replaced by ice 0.8–3.0 m thick. Variability in the calculated ocean-atmosphere heat flux and basal ice growth for ice-covered regions was primarily driven by changes in the surface air temperature as well as by the observed changes in the ice thickness distribution.

Heat fluxes during the fall periods were more sensitive to changes in the ice thickness distribution, with the eastern Arctic experiencing the greatest change in ice growth and heat flux due to changes in the ice thickness distribution. Taking variations in meteorological conditions into account, the fall period ocean-atmosphere heat fluxes were found to be greatly increased in 2005, 2006, and 2007 compared to 2003 due to thinning of the sea ice cover. The winter time heat fluxes were much more impacted by changes in the surface air temperature rather than changes in the ice thickness distribution. Although the mean ice thickness decreased over the 2004–2008 winter time periods, the winter effective insulation did not largely change until 2008 at which time it experienced a large decline of nearly 1 m in effective sea ice thickness. The large decline in the winter 2008 effective insulation is also associated with an increase in the heat flux after differences in meteorological forcings are taken into account, though this increase is not as prominent as that observed in the fall and is within the estimated uncertainty.

[55] For the whole of the Arctic Ocean, this study shows that increases in the net ocean-atmosphere heat output have occurred due to thinning and area (volume) loss of the Arctic sea ice cover. However, a remaining question is: what magnitude of changes to the surface air temperature have occurred due to this decrease in sea ice volume and associated increase in the ocean-atmosphere heat flux? Surface air temperatures in the Arctic are highly variable so quantifying the impact of a changing sea ice cover on surface air temperatures is difficult [Serreze and Francis, 2006]. Serreze *et al.* [2009] show that decreases in the areal extent of Arctic are tied to increased surface air temperatures for the 1979–2007 fall seasons, but that this effect is not largely present during the winter season. The increased surface air temperatures in the fall were found to be due to a surface heating source and attributed to an increased surface heat flux. This study shows that over the 2003–2008 time period losses in both ice thickness and areal coverage did indeed lead to an overall increase in the surface heat flux. Despite large losses in ice thickness and effective insulation, changes in ice areal coverage were found to be the dominant factor in impacting the surface heat flux. Most notably, the anomalously low areal coverage of sea in the fall of 2007 led to an ocean-atmosphere heat output nearly 3 times higher than that from previous years.

[56] Serreze *et al.* [2009] also note that slight warming may also be beginning to appear in the winter time. They state this may be due to delays in autumn freezeup, but eventually decreased ice extent and thickness in the winter will also begin to play a role. Delays in autumn freezeup have been observed by Markus *et al.* [2009]. However, this study shows that though there was a decrease in the mean thickness and amount of thick (>3 m) ice in the winter, these changes did not lead to a large change in the ocean-atmosphere heating rate since it is less sensitive to changes in the amount of

1021 thick ice. It appears that a surface warming signal associated  
 1022 with a thinning sea ice cover could just be beginning to  
 1023 emerge in the winter, but future observations will be required  
 1024 to determine whether this effect becomes stronger and more  
 1025 significant with time.

1026 [57] Overall, these results show that the decreasing volume  
 1027 of the Arctic sea ice cover has led to a decreasing ability to  
 1028 insulate the atmosphere from the relatively warm underlying  
 1029 ocean. This effect is currently most pronounced in the fall,  
 1030 with the winter being less affected as the ice has sufficiently  
 1031 thickened to a point where the ocean-atmosphere heat flux is  
 1032 less sensitive to changes in the ice thickness. These increased  
 1033 heat fluxes in the fall periods likely played a role in increasing  
 1034 surface air temperatures in the Arctic. Though this data set  
 1035 spans only 5 years, it was collected at a time when large losses  
 1036 in sea ice thickness and areal extent were observed. The  
 1037 continuation of large-scale sea ice thickness measurements  
 1038 from future airborne and satellite missions such as NASA's  
 1039 Operation IceBridge and the planned ICESat-2 mission, as  
 1040 well as ESA's CryoSat-2 mission, will be vital to under-  
 1041 standing future changes to the sea ice cover and its impact  
 1042 on the climate.

1043 [58] A major limitation in this study of the Arctic ocean-  
 1044 atmosphere heat flux and ice growth rate is the irregular time  
 1045 sampling and limited temporal availability of ICESat data.  
 1046 Future satellite altimetry missions will maintain year-round  
 1047 data collection for improved observation of year-to-year  
 1048 variations. For the currently available ICESat data, it would  
 1049 be useful to combine the observational data with model data  
 1050 using an assimilation approach. Doing so would enable a  
 1051 better understanding of reasons for the large losses in ice  
 1052 volume over the time period, how annual ice production was  
 1053 affected by the observed changes, and how an increased  
 1054 ocean-atmosphere heat flux from a reduced ice cover affected  
 1055 surface air temperatures throughout the whole of the Arctic.

1056 [59] **Acknowledgments.** The authors would like to thank two anyo-  
 1057 mous reviewers for their invaluable suggestions, which helped in improving  
 1058 the manuscript. The ECMWF data for this study are from the Research Data  
 1059 Archive (RDA), which is maintained by the Computational and Information  
 1060 Systems Laboratory (CISL) at the National Center for Atmospheric Research  
 1061 (NCAR). NCAR is sponsored by the National Science Foundation (NSF).  
 1062 The original data are available from the RDA (<http://dss.ucar.edu>) in data  
 1063 set number ds627.0. We also acknowledge NSIDC for providing the  
 1064 AMSR-E and ICESat data used in this study (<http://nsidc.org/>).

## 1065 References

1066 Ackerman, S. A., R. E. Holz, R. Frey, E. W. Eloranta, B. C. Maddux,  
 1067 and M. McGill (2008), Cloud detection with MODIS. Part II: Validation,  
 1068 *J. Atmos. Oceanic Tech.*, **25**, 1073–1086.  
 1069 Arctic Climate Impact Assessment (2005), *Arctic Climate Impact Assess-*  
 1070 *ment*, 1042 pp., Cambridge Univ. Press, Cambridge, U. K.  
 1071 Boé, J., A. Hall, and X. Qu (2009), Current GCMs' unrealistic negative  
 1072 feedback in the Arctic, *J. Clim.*, **22**, 4682–4695.  
 1073 Comiso, J. C., C. L. Parkinson, R. Gersten, and L. Stock (2008), Accelerated  
 1074 decline in the Arctic sea ice cover, *Geophys. Res. Lett.*, **35**, L01703,  
 1075 doi:10.1029/2007GL031972.  
 1076 Farrell, S. L., S. W. Laxon, D. C. McAdoo, D. Yi, and H. J. Zwally (2009),  
 1077 Five years of Arctic sea ice freeboard measurements from the Ice, Cloud  
 1078 and land Elevation Satellite, *J. Geophys. Res.*, **114**, C04008, doi:10.1029/  
 1079 2008JC005074.  
 1080 Giles, K. A., S. W. Laxon, and A. L. Ridout (2008), Circumpolar thinning  
 1081 of Arctic sea ice following the 2007 record ice extent minimum, *Geo-*  
 1082 *phys. Res. Lett.*, **35**, L22502, doi:10.1029/2008GL035710.  
 1083 Hack, J. J., B. A. Boville, B. P. Briegleb, J. T. Kiehl, P. J. Rasch, and  
 1084 D. L. Williamson (1993), Description of the NCAR Community Cli-

mate Model (CCM2), *Tech. Note TN-382+STR*, 108 pp., Natl. Cent.  
 for Atmos. Res., Boulder, Colo.  
 Key, J. R., R. A. Silcox, and R. S. Stone (1996), Evaluation of surface  
 radiative flux parameterizations for use in sea ice models, *J. Geophys.*  
*Res.*, **101**, 3839–3849.  
 Kovacs, A. (1996), Sea ice: Part II. Estimating the full-scale tensile, flexural,  
 and compressive strength of first-year ice, *Rep. 96-11*, Cold Reg. Res. and  
 Eng. Lab., Hanover, N. H.  
 Kurtz, N. T., T. Markus, D. J. Cavalieri, W. Krabill, J. G. Sonntag, and  
 J. Miller (2008), Comparison of ICESat data with airborne laser altimeter  
 measurements over Arctic sea ice, *IEEE Trans. Geosci. Remote Sens.*, **46**,  
 1913–1924.  
 Kurtz, N. T., T. Markus, D. J. Cavalieri, L. C. Sparling, W. B. Krabill,  
 A. J. Gasiewski, and J. G. Sonntag (2009), Estimation of sea ice thick-  
 ness distributions through the combination of snow depth and satellite  
 laser altimetry data, *J. Geophys. Res.*, **114**, C10007, doi:10.1029/  
 2009JC005292.  
 Kwok, R., and G. F. Cunningham (2008), ICESat over Arctic sea ice:  
 Estimation of snow depth and ice thickness, *J. Geophys. Res.*, **113**,  
 C08010, doi:10.1029/2008JC004753.  
 Kwok, R., G. F. Cunningham, H. J. Zwally, and D. Yi (2007), Ice, Cloud,  
 and land Elevation Satellite (ICESat) over Arctic sea ice: Retrieval of  
 freeboard, *J. Geophys. Res.*, **112**, C12013, doi:10.1029/2006JC003978.  
 Kwok, R., G. F. Cunningham, M. Wensnahan, I. Rigor, H. J. Zwally, and  
 D. Yi (2009), Thinning and volume loss of the Arctic Ocean sea ice cover:  
 2003–2008, *J. Geophys. Res.*, **114**, C07005, doi:10.1029/2009JC005312.  
 Laevastu, T. (1960), Factors affecting the temperature of the surface layer  
 of the sea, *Comment. Phys. Math.*, **25**, 128–134.  
 Lindsay, R. W. (1998), Temporal variability of the energy balance of thick  
 Arctic pack ice, *J. Clim.*, **11**, 313–333.  
 Liu, A. K., and D. J. Cavalieri (1998), Sea-ice drift from wavelet analysis  
 of DMSP SSM/I data, *Int. J. Remote Sens.*, **19**, 1415–1423.  
 Lupkes, C., T. Vihma, E. Jakobson, G. König-Langlo, and A. Tetzlaff  
 (2010), Meteorological observations from ship cruises during summer to  
 the central Arctic: A comparison with reanalysis data, *Geophys. Res.*  
*Lett.*, **37**, L09810, doi:10.1029/2010GL042724.  
 Manabe, S., and R. J. Stouffer (1980), Sensitivity of a global climate  
 model to an increase of CO<sub>2</sub> in the atmosphere, *J. Geophys. Res.*, **85**,  
 5529–5554.  
 Markus, T., J. C. Stroeve, and J. Miller (2009), Recent changes in Arctic  
 sea ice melt onset, freeze-up, and melt season length, *J. Geophys. Res.*,  
**114**, C12024, doi:10.1029/2009JC005436.  
 Maslanik, J. A., C. Fowler, J. Stroeve, S. Drobot, J. Zwally, D. Yi, and  
 W. Emery (2007), A younger, thinner Arctic ice cover: Increased  
 potential for rapid, extensive sea-ice loss, *Geophys. Res. Lett.*, **34**,  
 L24501, doi:10.1029/2007GL032043.  
 Maykut, G. A. (1978), Energy exchange over young sea ice in the central  
 Arctic, *J. Geophys. Res.*, **83**, 3646–3658.  
 Maykut, G. A. (1982), Large-scale heat exchange and ice production in the  
 central Arctic, *J. Geophys. Res.*, **87**, 7971–7984.  
 Maykut, G. A., and P. E. Church (1973), Radiation climate of Barrow,  
 Alaska, 1962–66, *J. Appl. Meteorol.*, **12**, 620–628.  
 Maykut, G. A., and D. K. Perovich (1987), The role of shortwave radiation  
 in the summer decay of a sea ice cover, *J. Geophys. Res.*, **92**, 7032–7044.  
 Maykut, G. A., and N. Untersteiner (1969), Numerical prediction of the  
 thermodynamic response of Arctic sea ice to environmental changes,  
*Doc. RM-6093-PR*, Rand Corp., Santa Monica, Calif.  
 Parkinson, C. L., and W. M. Washington (1979), A large-scale numerical  
 model of sea ice, *J. Geophys. Res.*, **84**, 311–337.  
 Pease, C. H. (1987), The size of wind-driven coastal polynyas, *J. Geophys.*  
*Res.*, **92**, 7049–7059.  
 Perovich, D. K., T. C. Grenfell, J. A. Richter-Menge, B. Light, W. B. Tucker  
 III, and H. Eicken (2003), Thin and thinner: Sea ice mass balance mea-  
 surements during SHEBA, *J. Geophys. Res.*, **108**(C3), 8050, doi:10.1029/  
 2001JC001079.  
 Persson, P. O. G., C. W. Fairall, E. L. Andreas, P. S. Guest, and  
 D. K. Perovich (2002), Measurements near the Atmospheric Surface  
 Flux Group tower at SHEBA: Near surface conditions and surface energy  
 budget, *J. Geophys. Res.*, **107**(C10), 8045, doi:10.1029/2000JC000705.  
 Rigor, I. G., J. M. Wallace, and R. L. Colony (2002), Response of sea ice to  
 the Arctic oscillation, *J. Clim.*, **15**, 2648–2663.  
 Rothrock, D. A., D. B. Percival, and M. Wensnahan (2008), The decline in  
 Arctic sea-ice thickness: Separating the spatial, annual, and interannual  
 variability in a quarter century of submarine data, *J. Geophys. Res.*,  
**113**, C05003, doi:10.1029/2007JC004252.  
 Semtner, A. J., Jr. (1976), A model for the thermodynamic growth of sea ice  
 in numerical investigations of climate, *J. Phys. Oceanogr.*, **6**, 379–389.  
 Serreze, M. C., and J. A. Francis (2006), The Arctic amplification debate,  
*Clim. Change*, **76**, 241–264.

- 1164 Serreze, M. C., A. P. Barrett, J. C. Stroeve, D. N. Kindig, and M. M. Holland 1186  
 1165 (2009), The emergence of surface-based Arctic amplification, *Cryosphere*, 1187  
 1166 3, 11–19. 1188
- 1167 Shine, K. P. (1984), Parameterization of shortwave flux over high albedo 1189  
 1168 surfaces as a function of cloud thickness and surface albedo, *Q. J. R.* 1190  
 1169 *Meteorol. Soc.*, 110, 747–764. 1191
- 1170 Stark, J. D., C. J. Donlon, M. J. Martin, and M. E. McCulloch (2007), 1192  
 1171 Ostia: An operational, high resolution, real time, global sea surface 1193  
 1172 temperature analysis system, paper presented at Oceans '07, Inst. of Electr. 1194  
 1173 and Electr. Eng., Aberdeen, U. K. 1195
- 1174 Steele, M., and T. Boyd (1998), Retreat of the cold halocline layer in the 1196  
 1175 Arctic Ocean, *J. Geophys. Res.*, 103, 10,419–10,435. 1197
- 1176 Stroeve, J., M. Serreze, S. Drobot, S. Gearheard, M. Holland, J. Maslanik, 1198  
 1177 W. Meier, and T. Scambos (2008), Arctic sea ice extent plummets in 1199  
 1178 2007, *EOS Trans. AGU*, 89(2), 13–14, doi:10.1029/2008EO020001. 1200
- 1179 Sturm, M., D. K. Perovich, and J. Holmgren (2002), Thermal conductivity 1201  
 1180 and heat transfer through the snow on the ice of the Beaufort Sea, 1202  
 1181 *J. Geophys. Res.*, 107(C21), 8043, doi:10.1029/2000JC000409.
- 1182 Wadhams, P., W. B. Tucker III, W. B. Krabill, R. N. Swift, J. C. Comiso, 1203  
 1183 and N. R. Davis (1992), Relationship between sea ice freeboard and draft 1204  
 1184 in the Arctic basin, and implications for ice thickness monitoring, *J. Geo-* 1205  
 1185 *phys. Res.*, 97, 20,325–20,334. 1206
- Warren, S. G., I. G. Rigor, N. Untersteiner, V. F. Radionov, N. N. Bryazgin, 1186  
 Y. I. Aleksandrov, and R. Colony (1999), Snow depth on Arctic sea ice, 1187  
*J. Clim.*, 12, 1814–1829. 1188
- Weeks, W. F., and O. S. Lee (1958), Observations on the physical proper- 1189  
 ties of sea ice at Hopedale, Labrador, *Arctic*, 11, 92–108. 1190
- Weller, G. (1972), Radiation flux investigation, *AIDJEX Bull.*, 14, 28–30. 1191
- Wentz, F., and T. Meissner (2000), AMSR ocean algorithm theoretical 1192  
 basis document, version 2, report, Remote Sens. Syst., Santa Rosa, Calif. 1193
- Wentz, F., and T. Meissner (2004), AMSR-E/Aqua Daily L3 Global 1194  
 Ascending/Descending .25 × .25 deg Ocean Grids, V002, October 1195  
 2003 to March 2008, [http://nsidc.org/data/ae\\_dyocn.html](http://nsidc.org/data/ae_dyocn.html), Natl. Snow 1196  
 and Ice Data Cent., Boulder, Colo. (Updated daily.) 1197
- Woodgate, R. A., T. Weingartner, and R. Lindsay (2010), The 2007 Bering 1198  
 Strait oceanic heat flux and anomalous Arctic sea-ice retreat, *Geophys.* 1199  
*Res. Lett.*, 37, L01602, doi:10.1029/2009GL041621. 1200
- Zwally, H. J., et al. (2002), ICESat's laser measurements of polar ice, atmo- 1201  
 sphere, ocean, and land, *J. Geodyn.*, 24, 405–445. 1202
- L. N. Boisvert, S. L. Farrell, N. T. Kurtz, T. Markus, and D. L. Worthen, 1203  
 Hydrospheric and Biospheric Sciences Laboratory, NASA Goddard Space 1204  
 Flight Center, 8800 Greenbelt Rd., MS 614.1, Greenbelt, MD 20771, USA. 1205  
 (nathan.t.kurtz@nasa.gov) 1206